Solid Earth Discuss., doi:10.5194/se-2017-23, 2017
Manuscript under review for journal Solid Earth
Discussion started: 30 March 2017

Solid Earth
Discussions
Open Access
EGU

Synchrotron FTIR imaging of OH in quartz mylonites

Andreas K. Kronenberg[1,*], Hasnor F.B. Hasnan[1,a], Caleb W. Holyoke III[1,b], and Richard D. Law[2], Zhenxian Liu[3], and Jay B. Thomas[4]

[1] Center for Tectonophysics, Department of Geology and Geophysics, MS 3115, Texas A&M University, College Station, TX, 77843-3115, USA

[2] Department of Geosciences, MC 0420, Derring Hall RM 4044, Virginia Polytechnic Institute and State University, Blacksburg, VA, 24061, USA

[3] Geophysical Laboratory, Carnegie Institution of Washington, 5251 Broad Branch Rd., NW Washington, D.C., 20015, USA

[4] Department of Earth Sciences, 204 Heroy Geology Laboratory, Syracuse University, Syracuse, NY, USA 13244, USA

[a] now at: Department of Advanced Geophysics, PETRONAS, Carigali Sdn. Bhd., PETRONAS Twin Towers, Kuala Lumpur City Centre, 50088 Kuala Lumpur, Malaysia

[b] now at: Department of Geosciences, University of Akron, Akron, OH, USA 44325-4101, USA

Solid Earth Discuss., doi:10.5194/se-2017-23, 2017
Manuscript under review for journal Solid Earth
Discussion started: 30 March 2017

Author Correspondence Information:

*Corresponding Author:
Andreas K. Kronenberg kronenberg@geo.tamu.edu 001 (979) 845-0132
FAX: 001 (979) 845-6162

Hasnor F.B. Hasnan hasnorfarhana@gmail.com

Caleb W. Holyoke III cholyoke@uakron.edu 001 (330) 972-7632 FAX:
001 (330) 972-7611

Richard D. Law rdlaw@vt.edu 001 (540) 231-6685 FAX: 001
(540) 231-3386

Zhenxian Liu zxliu@bnl.gov 001 (631) 344-7199

Jay B. Thomas jthom102@syr.edu 001 (315) 443-2672

Solid Earth Discuss., doi:10.5194/se-2017-23, 2017
Manuscript under review for journal Solid Earth
Discussion started: 30 March 2017

Solid Earth
Discussions
Open Access
EGU

Abstract

Methods of measuring OH absorption bands of fluid inclusions and hydrogen defects in deformed quartz-rich rocks at high spatial resolution are described, using synchrotron infrared IR radiation coupled with a Fourier transform infrared FTIR microscope, and applied to imaging OH in mylonites from the footwall of the Moine Thrust (from the Stack of Glencoul, NW Scotland Caledonides) and hanging wall of the Main Central Thrust (Sutlej Valley, Himalaya of NW India). Previous measurements of water in deformed quartzites using conventional FTIR instruments, through apertures of 50-100 μm for specimens ~100 μm in thickness have shown that water contents of larger grains vary from one grain to another. However, the non-equilibrium variations in water content between neighboring grains and within quartz grains cannot be interrogated further without greater measurement resolution, nor can water contents be measured in finely recrystallized grains without including absorption bands due to fluid inclusions, films, and secondary minerals at grain boundaries.

Synchrotron IR radiation is brighter and more collimated than offered by conventional FTIR globar light sources, and we have been able to distinguish and measure OH bands due to fluid inclusions, hydrogen point defects, and secondary hydrous mineral inclusions through an aperture of 10 μm for specimens > 40 μm thick. Doubly polished IR plates can be prepared with thicknesses down to 4-8 μm, but measurement of small OH bands is currently limited by strong interference fringes for samples < 25 μm thick, precluding measurements of water within individual, finely recrystallized grains. By translating specimens under the 10 μm IR beam by steps of 10 to 50 μm, using a software-controlled x-y stage, spectra have been collected over specimen areas of nearly 4.5 mm^2. Integrated absorbance of the broad OH band at 3400 cm^{-1} due to fluid inclusions was mapped and water content contoured, after subtracting the 3600 cm^{-1} band due to micas.

Solid Earth Discuss., doi:10.5194/se-2017-23, 2017
Manuscript under review for journal Solid Earth
Discussion started: 30 March 2017

Maps of the 3600 cm^{-1} band absorbance show concentrations of micas at grain grain boundaries, as well as finely dispersed mica inclusions within quartz grains.

Mylonitic Cambrian quartzites deformed under greenschist facies conditions in the footwall to the Moine Thrust exhibit a large and variable 3400 cm^{-1} band absorbance, and maps of water content corresponding to fluid inclusions show that inclusion densities correlate with deformation and recrystallization microstructures. Water contents of quartz grains in these mylonites are comparable to those of wet quartz varieties deformed in laboratory experiments. OH absorption bands of large clear quartz grains of mylonitic orthogneisses and paragneisses deformed under lower-upper amphibolite facies conditions in the hanging wall to the Main Central Thrust are much smaller, and dominated by sharp bands at 3595 cm^{-1} to 3379 cm^{-1} due to hydrogen point defects that appear to have uniform, equilibrium concentrations in the driest samples. The broad OH band at 3400 cm^{-1} in these rocks is much less common. The lack of detectable water in highly sheared Main Central Thrust mylonites offers a challenge to our understanding of quartz rheology. However, where water absorption bands can be detected and compared with deformation microstructures, OH concentration maps provide information on the histories of deformation and recovery, and evidence for the introduction and loss of fluid inclusions, and water weakening processes.

Keywords: FTIR Mapping, Water weakening, Dislocation Creep, Quartz

Solid Earth Discuss., doi:10.5194/se-2017-23, 2017
Manuscript under review for journal Solid Earth
Discussion started: 30 March 2017

1 Introduction

Quartz mylonites sheared at middle to lower levels of the continental crust exhibit microstructural and textural evidence of dislocation creep, a process that is widely believed to require water weakening in framework silicates. The effects of water on dislocation creep of quartz, including the nucleation, glide, climb and recovery of dislocations, and recrystallization are well known from: 1) experimental studies of natural crystals, in which water was introduced into grain interiors (e.g., Griggs, 1967; Blacic, 1975, 1981; FitzGerald et al., 1991), 2) studies of synthetic and natural quartz varieties with large initial water contents (e.g., Griggs and Blacic, 1965; Hobbs, 1968; Baeta and Ashby, 1970; Kekulawala et al., 1978; Kirby and McCormick, 1979; McLaren et al., 1983; Linker et al., 1984; Gerretsen et al., 1989; Muto et al., 2011; Holyoke and Kronenberg, 2013; Stünitz et al., in press), and 3) quartzites and polycrystalline quartz aggregates with water added or removed before or during experiments (e.g., Jaoul et al., 1984; Kronenberg and Tullis, 1984; Tullis and Yund, 1989; Hirth and Tullis, 1992; Gleason and Tullis, 1995; Post et al., 1996; Chernak et al., 2009). In addition to the parametric approach taken to study water weakening in deformation experiments, key insights into water weakening come from infrared IR spectroscopy of quartz samples that have been deformed in the lab under varying hydrothermal conditions, explicitly adding or removing water or changing the fugacity of H_2O at fixed temperature and/or strain rate. OH absorption bands characteristic of different hydrogen defects and forms of molecular water can be identified and their size used to determine concentration (e.g., Kats, 1962; Griggs and Blacic, 1965; Aines and Rossman, 1984; Aines et al., 1984; Stipp et al., 2006).

Water weakening in the continental crust is inferred because of the high laboratory strengths exhibited by quartz and feldspars in the absence of water (Griggs, 1967; Heard and Carter, 1968; Tullis and Yund, 1977, 1980; Tullis, 1983; Blacic and Christie, 1984) and the postulated effects of water on point defects and

Solid Earth Discuss., doi:10.5194/se-2017-23, 2017
Manuscript under review for journal Solid Earth
Discussion started: 30 March 2017

disruptions of fully linked Si-O bonds (Griggs, 1974; Hirsch, 1979; Hobbs, 1981; Paterson, 1989). With the advent of Fourier transform infrared FTIR spectroscopy and IR microscopes, water and hydrogen defects in naturally deformed quartz have been reported with OH contents of 300 ppm to >10,000 ppm (molar H/10^6 Si, Kronenberg and Wolf, 1990; Kronenberg et al., 1990; Nakashima et al., 1995; Gleason and DeSisto, 2008; Seaman et al., 2013; Finch et al., 2016), comparable to those required for water weakening in laboratory experiments. In small granitic shear zones deformed at greenschist conditions, water contents of quartz grains appear to correlate with finite strain (Kronenberg et al., 1990; Gleason and DeSisto, 2008), and in the much larger Median Tectonic Line of Japan, intragranular water contents increase towards its center (Nakashima et al., 1995). However, OH concentrations of quartz of granitic rocks deformed at higher temperatures can be much lower (20 - 100 ppm; Han et al., 2013; Kilian et al., 2016), with IR spectra dominated by small sharp OH bands of hydrogen point defects (Kilian et al., 2016) that are not thought to weaken quartz. Moreover, quartz water contents have been reported that show a trend of decreasing OH content towards the center of a high grade shear zone (Finch et al., 2016). Maps of OH content, constructed from FTIR spectra of deformed granitic rocks (Seaman et al., 2013) show compelling relationships between water content and microstructures generated during deformation, suggesting that water contents are reduced during recrystallization and partial melting.

Much as deformation microstructures and textures provide a link between our understanding of deformation mechanisms activated in deformation experiments at high laboratory strain rates and the mechanisms governing plasticity and creep of shear zones at low natural strain rates (Snoke et al., 1998; Heilbronner and Barrett, 2014), IR spectroscopy can provide a link between our understanding of water weakening in the lab and in nature. In this paper, we report on methods of FTIR spectroscopy to characterize OH absorption bands and image OH contents in quartz (and other nominally anhydrous minerals) at higher

Solid Earth Discuss., doi:10.5194/se-2017-23, 2017
Manuscript under review for journal Solid Earth
Discussion started: 30 March 2017

resolution than is possible using conventional instruments, coupling synchrotron IR radiation with FTIR spectroscopy. We then apply these methods to mylonitic quartzites in the footwall to the Moine Thrust in the NW Scotland and to mylonitic quartz-rich orthogneisses and paragneisses in the hanging wall to the Main Central Thrust in NW India. OH absorption bands are readily measured through an aperture of 10 μm for samples > 40 μm thick, sufficient to measure water contents in highly strained quartz grains (ribbons) and less deformed porphyroclasts and augen of the Moine Thrust mylonites. However, water contents of small individual recrystallized grains of the Moine Thrust mylonites could not be measured since spectra of doubly polished IR specimens < 25 mm thick display strong interference fringes. OH absorption bands can be measured for the larger grains of the Main Central Thrust mylonites, including original and recrystallized grains.

Images of intragranular water content in Moine Thrust and Main Central Thrust mylonites, based on contours of integrated absorbance of the broad OH band at 3400 cm^{-1} correspond to populations of fluid inclusions, and to deformation and recrystallization microstructures. Planar arrays of secondary fluid inclusions within quartz grain interiors provide evidence of increases in water during brittle microcracking, followed by crack healing and processes of fluid inclusion evolution and redistribution. Contoured integrated absorbances of the sharper band at 3600 cm^{-1} due to OH in micas show their spatial distributions at quartz grain boundaries and interiors.

2 Selected quartz mylonites

The quartz mylonites selected to test synchrotron FTIR spectroscopy and imaging of OH come from the footwall of the Moine Thrust at the Stack of Glencoul, NW Scotland (Christie, 1963; Law et al., 1986, 2010) and the hanging wall of the Main Central Thrust exposed in the Sutlej Valley, NW India (Law et al., 2013; Stahr,

Solid Earth Discuss., doi:10.5194/se-2017-23, 2017
Manuscript under review for journal Solid Earth
Discussion started: 30 March 2017

2013; Law, 2014). Both of these thrust faults are orogen-scale shear zones with penetrative deformation on the Moine Thrust accommodating shortening at the foreland edge of the Caledonian orogeny (e.g., Peach et al., 1907; Elliot and Johnson, 1980; Law et al., 1986, 2010; Butler, 2010; Law, 2010; Law and Johnson, 2010; Dewey et al., 2015) and penetrative shear strains on the Main Central Thrust accommodating southward directed extrusion/exhumation of the overlying Greater Himalayan slab (e.g., Grujic et al., 1996; Grasemann et al., 1999; Godin et al., 2006; Law et al., 2013). Mylonitic grain shape foliations are well developed in rocks of both fault zones and mineral stretching lineations are parallel to the fault transport directions. Deformation microstructures and textures of quartz in these mylonites indicate that dislocation creep was the predominant deformation mechanism involving both basal and prism slip systems, internal recovery and dynamic recrystallization.

Structural distances of samples below the Moine Thrust and above the Main Central Thrust, together with available information on deformation temperatures and temperatures/pressures of metamorphism, are summarized in Table 1. All samples from the footwall to the Moine Thrust are mylonitic Cambrian quartzites. Samples from the hanging wall to the Main Central Thrust on the NW Sutlej transect are penetratively deformed orthogneisses in which intensities of grain shape fabrics, traced downwards towards the thrust surface, increase (associated with the transition from grain boundary migration to subgrain rotation recrystallization) and dynamically recrystallized grain sizes decrease (Law et al. 2013; their fig. 6). Samples from the more hinterland-positioned Eastern Sutlej transect are less obviously foliated paragneisses with more granular textures due to extreme quartz grain boundary mobility. At a given distance above the Main Central Thrust, samples from the more hinterland positioned Eastern Sutlej transect have much larger recrystallized grain sizes than on the NW Sutlej transect (compare figs. 15 and 6 in Law et al. 2013).

Solid Earth Discuss., doi:10.5194/se-2017-23, 2017
Manuscript under review for journal Solid Earth
Discussion started: 30 March 2017

Mylonitic Cambrian quartzites in the footwall to the Moine Thrust at the Stack of Glencoul (Assynt region) display highly flattened relict grains aligned parallel to foliation, with grain shape aspect ratios up to 50:1 to 100:1 and smooth undulatory extinction between crossed polarizers that have been described as quartz ribbons (Bonney, 1883; Christie, 1960, 1963; Weathers et al., 1979; Law et al., 1986). At the margins of the larger quartz grains, more equant, finely recrystallized grains overprint these elongate high-strain grains, with the proportion of new to old grains increasing structurally upwards towards the Moine Thrust plane (Christie, 1960; Weathers et al., 1979; Law et al., 1986). Rare grains of feldspar and quartz aligned in "*mechanically strong*" orientations are relatively equant, and appear as augen or globular quartz grains. Quartz c-axes exhibit strong lattice preferred orientations in both deformed old grains and recrystallized grains, with symmetrical Type 1 (Lister, 1977) cross-girdle fabrics at distances > 150 mm beneath the thrust plane and increasingly asymmetric cross-girdle to single girdle fabrics closer to the thrust plane (Law et al., 1986, 2010). These fabrics reflect general flattening strains accommodated by quartz basal and prism slip, with variations in estimated flow vorticities and partitioning of strain between original and recrystallized grains (Law et al., 2010; Law 2010). Micas are highly aligned parallel to foliation, with coarse muscovite grains at quartz grain boundaries and fine, dispersed micas within quartz grain interiors. Optical microstructures show evidence of quartz recrystallization by bulge nucleation and subgrain rotation with relatively uniform mean recrystallized grain sizes of ~15 μm (Christie et al., 1954; Weathers et al., 1979). Microstructures imaged by transmission electron microscopy TEM show dense arrays of curved free dislocations, subgrain walls, and fine fluid inclusions that decorate dislocations (Weathers et al,, 1979; Ord and Christie, 1984). Earlier FTIR measurements of Moine Thrust mylonites from a number of locations in the Assynt region revealed large OH absorption bands characteristic of milky quartz with OH contents of 1500 to 7500 ppm (Kronenberg and Wolf, 1990).

Solid Earth Discuss., doi:10.5194/se-2017-23, 2017
Manuscript under review for journal Solid Earth
Discussion started: 30 March 2017

Quartz-rich Greater Himalayan Series orthogneisses and paragneisses in the hanging wall to the Main Central Thrust exposed in NW and Eastern Sutlej transects, respectively, include quartz mylonites, quartz-mica schists and quartz-garnet schists (Vannay and Grasemann, 1998; Grasemann et al., 1999; Law et al., 2013). Quartz grain shapes are not as highly elongate as observed in the Moine Thrust mylonites, owing to their extensive recrystallization, with mean grain sizes on the NW transect that vary with structural level from 200-250 μm (grain boundary migration microstructures) at ~1000 m above the Main Central Thrust to 75-95 μm at 200-750 m above the thrust, and 35-60 μm (dominantly subgrain rotation microstructures) at ~75 m above the thrust surface (Law et al., 2013). As noted above, quartz recrystallized grain sizes are much larger at a given structural height above the thrust plane on the hinterland-positioned Eastern transect with grain sizes commonly ranging from 250 - >1000 μm (0.25-1.0 mm) at ~ 25 m above the thrust to >1-2 mm at 200 m and higher above the thrust. Quartz grain interiors on the Eastern transect display mild undulatory extinction with highly aligned subgrain boundaries that give the appearance of chessboard extinction and irregular, non-planar grain boundaries that envelope neighboring mica grains, suggestive of high grain boundary mobilities at the time of peak metamorphism and deformation. Quartz *c*-axes show strong lattice preferred orientations with symmetrical and slightly asymmetrical cross-girdle fabrics on both transects, providing evidence of simultaneous basal and prism slip during plane strain deformation, with varying amounts of pure shear and simple shear (Law et al., 2013). Coarse-grained muscovite and biotite are highly aligned parallel to foliation, both at the boundaries of quartz grains and within quartz grain interiors.

While both the Moine Thrust and the Main Central Thrust mylonites were deformed by dislocation creep, their deformation temperatures were very different and the mechanisms of recrystallization, accommodating dislocation creep differ accordingly. Deformation temperatures for the Moine Thrust footwall mylonites at the Stack of Glencoul are estimated at between 300° and 350°C based on illite

Solid Earth Discuss., doi:10.5194/se-2017-23, 2017
Manuscript under review for journal Solid Earth
Discussion started: 30 March 2017

289 crystallinity (Johnson et al., 1985). Opening angles of *c*-axis fabrics measured
290 separately on old and recrystallized grains (Law et al., 2010) indicate far higher
291 apparent deformation temperatures using the Kruhl (1998) fabric opening angles
292 thermometer (390°-440°C and 475°-530°C, respectively) than are compatible with
293 their prehnite-pumpellyite to lower greenschist (chlorite) facies phyllosilicates
294 (Law, 2014). Deformation temperatures for Main Central Thrust hanging wall
295 mylonites range between ~535°-610°C on the NW Sutlej transect, using the Kruhl
296 (1998) opening angle thermometer, and ~ 610° - >735°C based on fabric opening
297 angles and petrologic constraints on the Eastern Sutlej transect (Table 1; Law et
298 al., 2013; Stahr, 2013).

299 Dynamic quartz recrystallization microstructures in the Moine Thrust
300 mylonites are similar to microstructures developed under experimental Regime II
301 creep conditions as defined by Hirth and Tullis (1992), with a combination of
302 bulge nucleation recrystallization (BLG) at grain boundaries and subgrain rotation
303 recrystallization (SGR) within quartz grain interiors, and they are consistent with
304 deformation under greenschist facies conditions (Stipp et al., 2002, 2010; Law,
305 2014). Quartz microstructures in the Main Central Thrust mylonites (particularly
306 on the Eastern Sutlej transect and at large distances above the thrust on the NW
307 transect) indicate more internal recovery and more extensive grain boundary
308 migration (GBM) than is apparent in the Regime III creep experiments of Hirth
309 and Tullis (1992). The microstructures are more similar to those observed by
310 Stipp et al. (2002; 2010) in quartz veins deformed at natural strain rates and the
311 equivalent of middle-upper amphibolite facies conditions (~550º-700ºC; see
312 review by Law, 2014).

313 The small recrystallized quartz grain sizes (16-9 μm), subgrain sizes, and
314 dislocation densities of the Moine Thrust footwall mylonites at the Stack of
315 Glencoul imply large differential stresses (40-250 MPa) during shearing
316 (Weathers et al., 1979; Ord and Christie, 1984); differential stresses of ~ 55-85
317 MPa are recalculated using these grain sizes and the recrystallized grain size

Solid Earth Discuss., doi:10.5194/se-2017-23, 2017
Manuscript under review for journal Solid Earth
Discussion started: 30 March 2017

piezometer of Stipp et al. (2006) modified by the stress correction of Holyoke and Kronenberg (2010). In contrast, quartz recrystallized grain sizes for Main Central Thrust mylonites on the NW Sutlej transect of 60-35 μm at 75 m above the thrust to 95-75 μm at 750-200 m above the thrust indicate lower differential stresses of 19-30 MPa and 13-16 MPa, respectively, using the Stipp et al. (2006) grain size piezometer, adjusted by the same stress correction (Francsis, 2012; Law et al., 2013). Flow stresses inferred for the Eastern Sutlej transect mylonites would presumably be even lower than for mylonites of the NW Sutlej transect, but their grain sizes are far greater than those encompassed by any experimental grain size piezometer.

3 Methods

IR spectroscopy has been an important tool for studying OH defects in nominally anhydrous minerals and, in coordination with deformation experiments, to study the effects of water and hydrogen defects on mechanical properties (e.g., Kats, 1962; Griggs and Blacic, 1965; Kekulawala et al., 1978, 1981; Aines and Rossman, 1984; Cordier and Doukhan, 1991; Mackwell and Kohlstedt, 1991; Bai and Kohlstedt, 1996; Kohlstedt et al., 1996). With the introduction of efficient FTIR spectrometers and IR microscopes, studies of intragranular water and hydrogen defects in naturally deformed rocks have been enabled using apertures of 50-100 μm (Kronenberg and Wolf, 1990; Nakashima et al., 1995; Gleason and DeSisto, 2008; Finch et al., 2016; Kilian et al., 2016) as well as FTIR mapping of OH contents (Seaman et al., 2013). Molecular water contents of naturally deformed quartz commonly have large grain-to-grain variations at this scale of observation, and it has not been possible to measure OH contents of dynamically recrystallized grains smaller than ~75-130 μm, without including absorption bands of fluid inclusions, fluid films, secondary minerals, and hydrogen species at grain boundaries.

Solid Earth Discuss., doi:10.5194/se-2017-23, 2017
Manuscript under review for journal Solid Earth
Discussion started: 30 March 2017

Synchrotron-generated IR radiation is much brighter (~1000x) than conventional globar sources of commercial FTIR instruments, and high quality IR spectra can readily be measured through small (10 μm) apertures (Lobo et al., 1999; Carr et al., 2008; Ma et al., 2013). By coupling synchrotron radiation to a FTIR instrument and IR microscope, OH absorption bands can be measured through a 10 μm aperture with higher signal-to-noise ratio than through a 100 μm aperture using a standard FTIR. We describe methods of preparing thin unsupported doubly polished IR samples and we compare IR spectra of quartz grains of deformed mylonites collected by FTIR spectroscopy using conventional and synchrotron IR sources. We also describe methods of scanning samples using a 10 μm IR beam, integrating absorbance of selected OH bands (due to fluid inclusions in quartz grains and micas at quartz grain margins and interiors) to form high-resolution images of OH in deformed and recrystallized mylonites. The ability to measure OH bands in finely recrystallized grains is not limited by aperture size or spectral quality for very thin (4-8 μm) samples. Rather, measurements for very thin IR plates are limited by internal reflections that give rise to interference fringes of increasing magnitude with decreasing sample thickness. In practice, measurements of the small OH bands of nominally anhydrous minerals are not possible for IR plate thicknesses of < 25 μm.

3.1 Preparation of IR plates

Doubly polished IR plates of uniform thickness were prepared perpendicular to foliation and parallel to lineation for Moine Thrust and Main Central Thrust mylonites. Images of large IR plates were collected using a high resolution (4000 dpi) Nikon slide scanner (Coolscan 8000 ED), with and without polarizing filters on both sides of the sample. Images of smaller IR plates were recorded with a Zeiss Axioplan 2 petrographic microscope and AxioCam HRc imaging system (Fig. 1). Image contrast was enhanced digitally (using Adobe Photoshop) for

Solid Earth Discuss., doi:10.5194/se-2017-23, 2017
Manuscript under review for journal Solid Earth
Discussion started: 30 March 2017

crossed-polarized light images of ultrathin samples with small optical retardations. Throughout the preparation of IR plates, impregnation of samples by epoxy or other insoluble resins was avoided to prevent the introduction of OH or CH absorption bands of mounting media, which might be difficult to distinguish from OH bands of samples. While central regions of the IR plates remain fragile, metal frames were mounted to IR plate extremities for mechanical support, to avoid catastrophic loss and facilitate handling.

Oriented rock chips were first mounted on a glass thin section plate using CrystalBond 509 (supplied by Aremco, NY) and a low-temperature hot plate. The top surfaces of samples were ground by hand against large glass plates using a sequence of silicon carbide (400 mesh size) and alumina powder slurries of decreasing particle size (600 mesh and 9.5 μm). Grinding with each grit size was carried out until the thickness of the sample, measured by a micrometer, was reduced by three times the grit dimension of the previous step (e.g., 3 μm grit was used to remove 3 x 9.5 μm = 29 μm). Samples were cleaned ultrasonically before advancing to the next grit size. Ground surfaces were then polished using polishing cloths (Buehler Texmet and Microcloth) mounted on high-speed laps and a sequence of alumina powder slurries with particle sizes of 3 and 0.3 μm, using the same measurement technique and testing the finish at each step by visual inspection.

Polished specimens were removed from the glass plate and remounted, this time on their polished surfaces, applying gentle pressure to sample centers to promote uniform thickness of the CrystalBond mounting medium (~20 μm). Sample plates were cut parallel to the first surface, and the second (cut) surface was ground and polished by the same methods outlined above. For the second surface, a micrometer was used to measure the compound thickness of sample, glass plate, and mounting medium, checking thickness at sample extremities, to adjust the grinding procedure for thickness uniformity. Sample thicknesses were determined from the compound sample-glass plate thickness, the glass plate

Solid Earth Discuss., doi:10.5194/se-2017-23, 2017
Manuscript under review for journal Solid Earth
Discussion started: 30 March 2017

thickness measured prior to mounting, and estimated CrystalBond layer thickness. In addition to micrometer measurements, sample thicknesses were tested during grinding, using interference colors for thicker samples (first order colors for quartz plates 50-90 μm thick) and maximum detectable birefringence (grey-white scale) while polishing ultrathin (< 20 μm) samples.

Before removing doubly polished samples from the glass thin section plate, metal frames were mounted to sample extremities using a thin bead of epoxy resin to provide support. For larger (> 10 mm) samples with thicknesses of 25 - 100 μm, metal frames made of Ni wire (1.15 mm diameter) were custom fit to each sample. For thin samples (< 25 μm), several metal frames normally used to mount TEM samples (3 mm outer diameter copper rings or slot rings with 1 x 2 mm internal dimensions; supplied by Ted Pella, Inc.) were mounted on each polished sample. Once the metal frames were attached and the epoxy hardened, samples were removed from the glass thin section over a low-temperature hot plate, and the CrystalBond resin removed using acetone.

Once quartz IR plates, 4 to 150 μm thick, are removed from the glass thin section plate, they are very fragile, and we found that they did not tolerate ultrasonic agitation. As a result, we soaked samples in acetone baths several times, dissolving CrystalBond resin for 30 minutes for each bath, exchanging the acetone in the beaker and repeating this procedure three times. Even without agitation, some samples did not survive when air bubbles were caught beneath them, leading to specimen warping and disintegration. However, with sufficient care, loss rates were low, and doubly polished IR plates were prepared without impregnating resins with thicknesses of 150 μm to 4 - 8 μm.

3.2 FTIR spectroscopy

IR absorption spectra were collected for quartz mylonites of varying plate thickness using a Nicolet Magna 560 FTIR with Omnic software, a conventional

Solid Earth Discuss., doi:10.5194/se-2017-23, 2017
Manuscript under review for journal Solid Earth
Discussion started: 30 March 2017

globar source and NicPlan IR microscope (at Texas A&M University), and using a Bruker Hyperion FTIR spectrometer, OPUS software, and IR microscope at the U2A synchrotron beamline of the National Synchrotron Light Source NSLS I (at Brookhaven National Laboratory). Both the Nicolet and Bruker instruments make use of liquid nitrogen-cooled MCT detectors capable of absorbance measurements at wavenumbers of 7400 to 400 cm^{-1}, but we did not routinely store data beyond 4000 to 2000 cm^{-1}. We chose to collect spectra at a wavenumber resolution of 4 cm^{-1} on both instruments, compiling 512 scans for each spectrum, adjusting to larger numbers of scans with the Nicolet FTIR when needed to reduce noise in the spectrum. For purposes of comparison, all absorbances shown in spectra for quartz grains of varying thickness have been normalized to a common thickness of 1 mm.

Representative IR spectra of individual quartz grains from Moine Thrust and Main Central Thrust samples measured with the Nicolet FTIR (100 μm aperture) exhibit OH absorption bands of variable size and character (Fig. 2). Moine Thrust quartz spectra show a broad OH stretching band at 3400 cm^{-1} of large but variable magnitude (Fig. 2a), characteristic of molecular water in fluid inclusions of milky quartz (Kekulawala et al., 1978; Aines and Rossman, 1984; Stünitz et al., in press). In addition to this absorption band, some quartz grains from Moine Thrust samples show an additional absorption band (or subtle shoulder) at ~3600 cm^{-1} (Fig. 2b) due to fine scale micas (sometimes visible optically and sometimes too fine to resolve) dispersed within quartz grains. Main Central Thrust quartz spectra tend to have smaller OH absorption bands (Fig. 2c), with some grains showing small sharp bands at 3595, 3482, 3431, 3408, and 3379 cm^{-1} due to hydrogen interstitial defects (Kats, 1962; Aines and Rossman, 1984) and less common grains with a larger broad band at 3400 cm^{-1}. Finely dispersed micas are less common in these coarser-grained mylonites, but some quartz grains also exhibit a 3600 cm^{-1} OH band due to micas (Fig. 2d).

Solid Earth Discuss., doi:10.5194/se-2017-23, 2017
Manuscript under review for journal Solid Earth
Discussion started: 30 March 2017

462 Aside from differences in the Nicolet and Bruker FTIR instruments and
463 software, the most significant difference between these facilities is the IR source,
464 so that OH absorption measurements with the Nicolet FTIR and its conventional
465 IR source could not practically be made with apertures < 50-100 μm, while OH
466 absorption bands could routinely be made with the Bruker FTIR and synchrotron
467 IR source through a 10 μm aperture. In both cases, the IR sources are nearly
468 isotropic, leading to differences in those OH absorption bands that are dichroic in
469 quartz and mica grains of varying orientation. Small sharp OH bands due to
470 hydrogen interstitials of quartz between 3595 cm^{-1} and 3379 cm^{-1} absorb most
471 strongly for vibrational directions perpendicular to the quartz *c* axis (Kats, 1962),
472 and these bands vary according to the c-axis orientation of each quartz grain
473 relative to the unpolarized IR beam. OH absorption bands at ~3600 cm^{-1} of micas
474 are strongly dichroic (Beran, 2002), and they vary according to mica grain
475 orientations relative to the unpolarized IR beam. However, the primary OH band
476 of interest for water-weakening of milky quartz, at 3400 cm^{-1}, is broad and
477 isotropic (Kekulawala et al., 1978; Aines et al., 1984), and associated with finely
478 dispersed fluid inclusions. Variations in absorbance of this band for neighboring
479 quartz grains represent real variations in water content and not variations in quartz
480 grain orientation.
481 IR microscope stages are not purged as effectively as sample chambers of
482 FTIR spectrometers that are evacuated or operate at positive nitrogen pressures,
483 and some of our spectra show evidence of atmospheric contamination. We
484 attempted to minimize absorption bands due to H_2O vapor and CO_2 by making
485 spectral measurements of samples and the background (without the sample in the
486 IR beam) at similar times after the last sample change or disturbance at the
487 microscope stage. However, atmospheric absorptions were not always cancelled
488 completely, with the appearance of "noise" between 3940 and 3420 cm^{-1} due H_2O
489 vapor vibrations (Fig. 2a, Grain 26; Fig. 2b, Grains 11B and 39) and absorptions at
490 2337 and 2361 cm^{-1} due to CO_2, which were either under- or over-corrected by

Solid Earth Discuss., doi:10.5194/se-2017-23, 2017
Manuscript under review for journal Solid Earth
Discussion started: 30 March 2017

subtracting the measured background (Fig. 2a, Grain 26 and Fig. 2b, Grains 11B and 39, and Fig. 2d, Grain 4 show examples of CO_2 band under-correction; Fig. 2c, all grains show negative deflections at 2337 and 2361 cm^{-1} due to over-correction of CO_2 absorptions).

Direct comparisons of intragranular water of a given quartz grain using the two FTIR facilities and a common aperture size could not be made because of 1) the poor signal-to-noise ratio of spectral measurements through a 10 μm aperture with the broad globar IR radiation, and 2) the inability to make spectral measurements for a 100 μm-apertured area with the narrow synchrotron IR beam (which is not much broader at the microscope stage than the 10 μm aperture). Samples with uniform OH contents might serve as standards to compare OH absorption bands for different spectrometers, irrespective of aperture size, but our observations indicate that OH contents of the quartz grains in the mylonites we measured are highly variable. Measurements through finer apertures led to larger variances in OH absorption bands, within grains as well as between neighboring grains.

We also observed larger amplitude interference fringes in spectra measured with the synchrotron IR source than those observed in spectra measured with the globar IR source for a given sample. These fringes are caused by internal reflection within doubly polished, parallel-sided IR plates, and they have larger magnitudes for the highly collimated IR synchrotron beam than for the broad, confocal globar IR radiation.

3.3 Interference fringes

The appearance of interference fringes in spectra can be useful to determine the optical path length in thin samples, as long as their amplitude is small compared with vibrational absorption bands of interest, or they are distinguishable from absorption bands by their wavenumber spacing. Interference fringes are present in

Solid Earth Discuss., doi:10.5194/se-2017-23, 2017
Manuscript under review for journal Solid Earth
Discussion started: 30 March 2017

520 many spectra we collected for quartz mylonite plates (Fig. 2c, Grains 1 and 8), that
521 are of manageable size for our thicker samples and problematic for thinner
522 samples.
523 Interference fringes were routinely observed for all samples measured with
524 synchrotron IR radiation and the Bruker FTIR instrument. We therefore made use
525 of these fringes to determine local sample plate thicknesses. For sample plates
526 with large interference fringes, we attempted to reduce their size by tilting samples
527 by 45° in the IR beam or using a Cassegrain objective lens with large numerical
528 apertures (0.6). However, neither of these methods was effective in reducing
529 amplitudes of some of the very large interference fringes sufficiently to detect
530 small OH absorption bands. We had greater success reducing interference fringes
531 by fitting them where the baseline was free of absorption bands, using DatLab
532 software (similar to fringe modeling of Clark and Moffatt, 1978; Pistorius and
533 DeGrip, 2004; Konevskikh et al., 2015), and subtracting the model fringes from
534 the spectral data. This improved the quality of spectra when interference fringes
535 had modest amplitudes, but interference fringes for thin samples were very large
536 and resulting backgrounds sufficiently irregular that we could not resolve small
537 OH absorption bands.
538
539 **3.4 IR plate thickness and OH absorbance determinations**
540
541 IR plate thicknesses were determined by focusing on imperfections in the top and
542 bottom specimen surfaces, and recording the numerical graduation on the focusing
543 knob of the Nicolet FTIR microscope for each surface. The focusing knob
544 graduations were calibrated for vertical translation using the same procedure for a
545 thick (~3 mm) quartz specimen that had been measured with a micrometer.
546 Local IR plate thicknesses were also determined from interference fringes
547 measured in spectra collected with the synchrotron-Bruker FTIR microscope
548 system, where thickness t is given by

Solid Earth Discuss., doi:10.5194/se-2017-23, 2017
Manuscript under review for journal Solid Earth
Discussion started: 30 March 2017

549

550 $$t = 1 / (2 n \delta\upsilon) \quad (1)$$

551

552 where n is the mean refractive index of quartz (n = 1.55) and $\delta\upsilon$ is the measured
553 peak-to-peak fringe spacing (Stuart et al., 1996; Griffiths and de Haseth, 2007).
554 The two measures of thickness were in agreement within resolution (~ 5%) for a
555 given IR plate and location within the specimen, with thick IR specimens (~100
556 μm) showing real variations in local thickness of ± 10 μm and thin samples
557 varying in local thickness from 4 to 8 μm.
558 IR spectra were collected and integrated absorbances of OH bands were
559 measured above an assumed straight-line background, where backgrounds were fit
560 and integration limits were chosen at the same wavenumber values, from ~3705
561 cm^{-1} to 2880 cm^{-1} for OH bands of quartz grains and ~3702 cm^{-1} to 3544 cm^{-1} for
562 OH bands of micas (Fig. 3a). We have confidence in our ability to separate OH
563 absorption bands due to fluid inclusions in quartz and due to micas in Moine
564 Thrust samples, because IR spectra of coarse muscovite grains in Moine Thrust
565 mylonites consist of a single OH absorption band at 3620 cm^{-1} (Fig. 3b). This
566 strong OH stretching band is well known from multiple spectroscopic studies of
567 muscovite (Beran, 2002; Tokiwai and Nakashima, 2010a,b; Kallai and Lapides,
568 2015).
569 Our ability to distinguish OH absorbance due to fluid inclusions and micas
570 in Main Central Thrust samples, by contrast, is poor. In addition to the primary
571 OH absorption bands of muscovite (Fig. 3c) and biotite (Fig. 3d) grains at 3638
572 cm^{-1} and 3614 cm^{-1}, respectively, Main Central Thrust muscovite spectra show
573 smaller OH bands at 3815, 3311, 3146, and 3035 cm^{-1} and biotite spectra show
574 shoulders at both sides of the primary OH absorption band (at ~3679 cm^{-1} and
575 ~3561 cm^{-1}) and significant OH bands at 3258, 3043, and 2829 cm^{-1}. All of these
576 OH bands are anisotropic, and complexly so. OH band absorbances of micas will
577 therefore vary with crystallographic orientation within an unpolarized IR beam.

Solid Earth Discuss., doi:10.5194/se-2017-23, 2017
Manuscript under review for journal Solid Earth
Discussion started: 30 March 2017

578 The primary OH band of Main Central Thrust muscovite at 3638 cm^{-1}, measured
579 in polarized IR radiation, is strongest when the vibration direction E is parallel to
580 the basal plane (001), consistent with idealized hydrogen positions in dioctahedral
581 micas and the polarization of OH bands normally reported for muscovite (Beran,
582 2002). However, our polarized IR measurements of muscovite OH bands at 3311,
583 3146, and 3035 cm^{-1} indicate that they are more nearly isotropic. The primary OH
584 band of Main Central Thrust biotite grains at 3614 cm^{-1} is strongest when E is
585 perpendicular to (001), consistent with hydrogen positions of trioctahedral micas
586 and OH band polarizations observed for phlogopite (Beran, 2002). However, the
587 OH bands at 3258, 3043, and 2829 cm^{-1} are only weakly polarized and in the
588 opposite sense of the primary 3614 cm^{-1} band.
589 As a result, we only feel confident in our determinations of OH
590 absorbances of quartz grains in Main Central Thrust mylonites (Fig. 2c), when
591 mica inclusions are absent (3600 cm^{-1} band is undetectable). When the 3600 cm^{-1}
592 band is present (Fig. 2d), we cannot readily interpret absorption bands of
593 molecular water or hydrogen defects in quartz; at best, quartz OH contents are
594 overestimated.
595 Integrated absorbances of OH bands of quartz were used to determine OH
596 contents based on the Beer-Lambert relation (Stuart et al., 1996; Griffiths and
597 Haseth, 2007),
598
599 $$A = k\ c\ t \qquad (2)$$
600
601 where integrated absorbance Δ (= A/t, determined in cm^{-2}), is related to the
602 concentration c of OH, assuming that k for the broad isotropic OH band at 3400
603 cm^{-1} due to fluid inclusions in milky quartz is the same as for the broad isotropic
604 OH absorption band of molecular water in wet synthetic quartz (Aines et al.,
605 1984);
606

Solid Earth Discuss., doi:10.5194/se-2017-23, 2017
Manuscript under review for journal Solid Earth
Discussion started: 30 March 2017

607 $$c \text{ (in molar ppm, OH/10}^6 \text{ Si)} = 1.05\ \Delta \text{ (in cm}^{-2}\text{)}. \quad (3)$$

608

609 To the extent that spectra include sharp OH absorption bands due to hydrogen
610 point defects, this calibration will overestimate OH concentrations due to H
611 interstitials, given that the value of k for these bands is larger than for molecular
612 water (Kats, 1962; Thomas et al., 2009) for quartz grains oriented for maximum
613 OH absorbance (vibrational directions perpendicular to the c axis). However,
614 apparent OH concentrations due to H interstitials will appear smaller for quartz
615 grains oriented for minimum OH absorbance in unpolarized IR radiation. These
616 errors are not serious for quartz grains with large molecular water contents that
617 dominate over hydrogen point defect concentrations. However, we expect that our
618 determinations of OH concentrations for dry quartz grains (< 100 ppm) with
619 spectra dominated by sharp dichroic OH bands are not as accurate as for wet
620 quartz grains with spectra dominated by isotropic broad OH bands. We also
621 acknowledge that the calibration for molecular water absorption of synthetic
622 quartz used here differs from the calibration of the 3400 cm^{-1} OH band absorbance
623 reported by Stipp et al. (2006) for milky quartz grains with fluid inclusions. If this
624 alternative calibration is correct, OH contents reported here are smaller by a factor
625 of 0.56. The calibration of Stipp et al. (2006) is based on FTIR measurements of
626 individual grains of a pure quartzite and independent Karl Fischer titration of
627 disaggregated quartz particles, and we do not understand the source of
628 discrepancies in absorbance calibrations.

629 Integrated absorbances Δ (A/t in cm^{-2}) were also measured for the 3600 cm^{-1}
630 OH band of micas but no attempt was made to convert these to OH
631 concentrations. Muscovite grains of Moine Thrust samples show simple OH
632 absorption spectra with one prominent band at ~3600 cm^{-1} (Fig. 3b), but integrated
633 absorbances for this band cannot be converted to muscovite (or OH) content
634 without polarized IR spectral measurements and detailed knowledge of muscovite
635 grain orientations. Integrated absorbances of OH bands of muscovite and biotite

Solid Earth Discuss., doi:10.5194/se-2017-23, 2017
Manuscript under review for journal Solid Earth
Discussion started: 30 March 2017

grains in Main Central Thrust samples at wavenumbers of 3800 cm^{-1} to 2830 cm^{-1} are more complicated to interpret. In addition to the need for polarized IR measurements and grain orientation information, integrated OH absorbances due to unseen (below optical resolution) mica inclusions will depend on whether the micas consist of muscovite or biotite, or both.

3.5 Mapping OH absorption bands

Integrated areas of OH were measured as a function of spatial x and y dimensions within IR plates measured on the Bruker FTIR system, separating absorbances of OH bands due to fluid and mica inclusions to the extent that this was possible. Samples were translated under the 10 μm IR beam using a motorized x-y stage, controlled by OPUS software, and spectra were collected for each translation step, usually moving the stage by 10 μm. In those cases where we mapped coarse-grained samples over large regions (up to ~4.5 mm^2), we increased the step spacing to 30 or 50 μm, in order to limit total step-scan measurement times and the number of required steps (our software version could not compile > 99 steps in a single row of measurements). Integrated absorbance measurements were made over 3705 - 2880 cm^{-1} (to include the 3400 cm^{-1} broad band of milky quartz) and 3702 - 3544 cm^{-1} (to determine the 3600 cm^{-1} mica band) for each scanned area (compiling absorbance measurements for 660 to 4950 spectra). The integrated absorbances of the 3600 cm^{-1} mica band were subtracted from the first of the two integrated absorbances, saving the result as a representative measure of the OH bands of molecular water and hydrogen defects of quartz.

Given that the same IR background was used to reference all spectral measurements made during x-y mapping of OH bands, long step-scan mapping projects were susceptible to changes in aperture and condenser lens centering, IR beam drift and beam outages while the synchrotron ring was refilled. As a result, we modified our IR absorbance measurement methods for step-scan mapping to

Solid Earth Discuss., doi:10.5194/se-2017-23, 2017
Manuscript under review for journal Solid Earth
Discussion started: 30 March 2017

obtain reasonably accurate integrated absorbances of broad OH bands without requiring high resolution or precision measurements of small, sharp OH bands, with the goal of limiting total measurement times.

IR spectra used to map OH bands were made at a wavenumber resolution of 8 cm^{-1}, reducing the interferometer mirror translation times with no detectable degradation in integrated absorbance measurements. More significantly, we reduced the number of scans to measure each IR spectrum from 512 to just 16, resulting in measurement times for each spectrum of only ~10 s, including the time for stage translation. This number of scans was chosen on the basis of tests for a given quartz grain of Moine Thrust sample SG-10 with an absorbance of 36 cm^{-1} measured over 3705 - 2880 cm^{-1} (or Δ = 3000 cm^{-2} for a sample thickness t of 120 μm), determining integrated absorbances for spectra compiled for 512, 256, 128, 64, 32, 16, and 8 scans. Integrated absorbances of the broad 3400 cm^{-1} band varied by less than 4% for measurements made with 512 - 32 scans, while the absorbance measurements for 16 and 8 scans were within 8% and 12%, respectively, of the mean of the other determinations. OH maps were thereby constructed for sample areas of 0.066 mm^2 (22 x 30 = 660 spectra) to nearly 4.5 mm^2 (50 x 99 = 4950 spectra) requiring measurement times of 110 minutes to nearly 14 hours, respectively. The larger step-scan maps include some poor spectral data corresponding to beam drift or interruption of radiation; these spectra were identified and removed from the data set.

Maps of integrated OH absorbance were contoured (using SigmaPlot) to form images of water contents and micas, and superposed on optical micrographs of the measured regions, to look for correlations between OH content and microstructure. OH contents of quartz, due primarily to the broad 3400 cm^{-1} OH band of fluid inclusions and secondarily to sharp hydrogen defect bands, were mapped as molar ppm ($OH/10^6Si$), while the OH absorption band at ~3600 cm^{-1} due to micas was mapped in units of integrated absorbance (cm^{-2}). Logarithmic contour intervals of $\log_{10}(OH/10^6Si)$ were chosen to image water contents in quartz

Solid Earth Discuss., doi:10.5194/se-2017-23, 2017
Manuscript under review for journal Solid Earth
Discussion started: 30 March 2017

694 over a wide range of concentrations, and to provide visual images of water
695 distributions at low (and high) values. OH contents were contoured in color with
696 blue (and other cool colors) corresponding to large water contents, and red (and
697 other warm colors) corresponding to low water contents. Logarithmic contours
698 were also chosen to image distributions of micas, plotting $\log_{10}(\Delta$ in $cm^{-2})$ for the
699 integrated absorbance of the ~3600 cm^{-1} OH band, using a similar key for the
700 contour interval, where cool colors correspond qualitatively to high mica contents
701 and warm colors correspond to low mica contents.
702
703 **4 Results**
704
705 Synchrotron radiation coupled with the FTIR spectrometer and microscope at the
706 NSLS I has enabled spectral measurements for sampling volumes that are smaller
707 by a factor of 100 than is possible with a conventional FTIR microscope system.
708 OH band measurements for quartz through a 10 μm aperture are comparable to
709 OH band measurements made using a conventional FTIR spectrometer-
710 microscope system through a 100 μm aperture. The ability to measure OH bands
711 of individual recrystallized quartz grains is currently limited by IR plate thickness,
712 not because of signal-to-noise problems, but because of internal reflections in
713 ultrathin IR plates. Water contents of quartz grains, and OH contents associated
714 with micas and other hydrous phases, can be measured spatially by translating
715 samples under the 10 μm-apertured beam and contouring integrated OH
716 absorbance over chosen wavenumber intervals. High-resolution images, formed
717 in this way, can be compared with optical deformation microstructures, providing
718 a means of studying the role of water in deformation and changes in water content
719 during deformation and recrystallization.
720
721 **4.1 Synchrotron FTIR Measurements**
722

Solid Earth Discuss., doi:10.5194/se-2017-23, 2017
Manuscript under review for journal Solid Earth
Discussion started: 30 March 2017

IR spectra of quartz in Moine Thrust and Main Central Thrust samples measured with the synchrotron-FTIR system through a 10 μm aperture exhibit OH absorption bands of similar character at the same wavenumbers as measured for samples of the same thickness (~100 μm) using a conventional FTIR spectrometer-microscope system through a 100 μm aperture. OH bands of Moine Thrust quartz grains generally include a large broad absorption band at 3400 cm^{-1} due to dispersed fluid inclusions, with some grains showing a secondary absorption band at 3600 cm^{-1} due to mica inclusions (Fig. 4a), just as those measured for larger sampling volumes (Fig. 2a, b). Given the more intense IR radiation of the synchrotron source, we did not encounter any losses in spectral quality due to signal-to-noise ratios for the smaller sample volumes measured. However, interference fringes were more apparent using the synchrotron-FTIR microscope system associated with internal reflections from the parallel-sided IR plates and the lower divergence of the synchrotron beam. Synchrotron FTIR measurements of Main Central Thrust samples through a 10 μm aperture show the same sharp OH bands due to hydrogen point defects as measured through a 100 μm aperture. With the exception of some unusual grains, broad OH bands at 3400 cm^{-1} in Main Central Thrust samples are small to negligible.

Integrated absorbances of the broad 3400 cm^{-1} OH band measured with a 10 μm aperture are highly variable spatially, yielding water contents for individual spots within quartz grains for a given Moine Thrust sample (SG-10) of 280 to 9000 ppm, with a comparable mean (2430 ppm) but more variance among individual measurements than measured with a 100 μm aperture (from 1130 to 8590 ppm for 45 measurements). For dry Main Central Thrust samples (S09-71B), OH contents of quartz measured using a small (10 μm) aperture varied from 50 to 300 ppm while OH contents measured with the larger (100 μm) aperture varied from 85 to 240 ppm. For unusually wet Main Central Thrust samples (S09-35), OH contents of quartz measured using a small (10 μm) aperture varied from 150 to 7500 ppm while OH contents measured with the larger (100 μm) aperture

Solid Earth Discuss., doi:10.5194/se-2017-23, 2017
Manuscript under review for journal Solid Earth
Discussion started: 30 March 2017

752 varied from 160 to 4620 ppm. The variations in size of sharp OH bands associated
753 with hydrogen point defects, by comparison, are much smaller. The sizes of these
754 dichroic absorption bands may be explained by differing quartz grain orientations
755 without calling upon any variations in hydrogen point defect concentrations
756 (Thomas et al., 2009).
757
758 **4.2 Limits of IR plate thickness**
759
760 IR spectra of quartz were measured through a 10 μm aperture, varying sample
761 plate thickness from ~100 μm to 4-8 μm, with the hope that we might be able to
762 measure the OH bands of individual recrystallized grains in ultrathin IR plates.
763 Owing to the coarse recrystallized grain sizes of Main Central Thrust mylonites,
764 we were able to measure IR spectra of most quartz grains in these samples for
765 plate thicknesses of >50 μm. However, our IR measurements of individual grains
766 in Moine Thrust samples (with recrystallized grains of ~10-15 μm) are limited to
767 larger porphyroclastic and deformed ribbon quartz grains. While the signal-to-
768 noise ratio of our measurements continue to be acceptable to measure the small
769 OH absorption bands in very thin IR plates, interference fringes increase in size as
770 the IR plate thickness t is decreased. Interference fringes become very large at $t <$
771 25 μm and OH bands cannot be detected at t = 13 μm and 6.5 μm (Fig. 4b, c).
772 The magnitude of interference fringes can be modified by tilting the
773 sample within the IR beam and increasing the numerical aperture of the
774 Cassegrain objective on the IR microscope. However, with peak-to-trough fringe
775 magnitudes 10^4 greater than the OH bands in our mylonite samples, the modest
776 reductions in fringe amplitude realized by these methods are not significant for the
777 measurement of OH absorptions. Our efforts to model interference fringes were
778 largely successful, reducing their magnitudes by a factor of ~100, but the resulting
779 backgrounds were not flat enough at the scale of the known OH absorption bands
780 of the Moine Thrust (or Main Central Thrust) samples to allow absorption band

Solid Earth Discuss., doi:10.5194/se-2017-23, 2017
Manuscript under review for journal Solid Earth
Discussion started: 30 March 2017

781 measurements for our thinnest sample plates. Interference fringes vary in
782 magnitude according to IR plate thickness, surface polish, and scattering by
783 internal flaws, but OH absorption bands could only be measured for samples of
784 ~40 μm thickness or greater.
785
786 **4.3 Optical microstructures and plate thickness**
787
788 Although the painstaking efforts to prepare ultrathin IR plates were not rewarded
789 by spectral measurements of OH content within individual, finely recrystallized
790 grains, optical imaging of deformation and recrystallization microstructures in
791 ultrathin samples was improved over that using conventional thin sections.
792 Optical microstructures of 100 μm-thick IR plates are poorly resolved by
793 comparison with those imaged in 30 μm-thick sections (Fig. 1c, d), with
794 interference colors that reflect greater optical retardation, grain boundaries that are
795 not as clearly defined, and greater numbers of overlapping grains. Remarkably,
796 ultrathin IR plates of quartz mylonites, just 4-8 μm thick (Fig. 1f), continue to
797 exhibit contrast between grains and within grains, with first-order black to grey
798 birefringence that can be enhanced by increasing image contrast.
799 High magnification optical micrographs of ultrathin Moine Thrust
800 mylonites reveal microstructures (Fig. 5) that correspond better to TEM
801 observations (Weathers et al., 1979; Ord and Christie, 1984) than to optical
802 microstructures of conventional thin sections. While highly flattened ribbon
803 quartz grains observed in 30 μm sections show smoothly varying undulatory
804 extinction, ultrathin sections exhibit well developed subgrains within grain
805 interiors, with sharply defined changes in extinction marking the locations of
806 distinct subgrain walls (Fig. 5a). Prior TEM of Moine Thrust mylonites revealed
807 significant densities of free dislocations that have been associated with smooth
808 changes in extinction. However, TEM observations also show dense, sharply
809 defined subgrain walls (Weathers et al., 1979; Ord and Christie, 1984) that are

Solid Earth Discuss., doi:10.5194/se-2017-23, 2017
Manuscript under review for journal Solid Earth
Discussion started: 30 March 2017

often not resolved as optical microstructures of normal thin sections. These observations suggest that ultrathin sections may be useful to distinguish smooth changes in extinction (due to free dislocations and strains internal to subgrains) from discrete changes in extinction of overlapping and neighboring subgrains.

Recrystallized grains are apparent at some sutured grain boundaries in Moine Thrust samples (Fig. 5a) with grain sizes that are significantly smaller than the dimensions of subgrains within the ribbon quartz grains. Microstructures of these new grains suggest that they form by grain boundary bulge mechanisms. Newly recrystallized grains surrounding other grains (Fig. 5b) have sizes in common with nearby subgrains, and microstructures suggest that these recrystallized grains develop by subgrain rotation. While prior optical examination of Moine Thrust mylonites using 30 μm thin sections has led to the conclusion that both BLG and SGR recrystallization were important during deformation (Law, 2014), quantitative evaluations of these processes and their contributions to dislocation creep could be improved by the higher microstructural resolution offered by ultrathin sections.

4.4 High-resolution imagining of OH

By translating IR plates under the 10 μm apertured IR beam and measuring spectra over many steps (spaced by 10 to 50 μm) we were able to compile integrated absorbances over spatial areas of up to 4.455 mm^2 (50 x 99 = 4950 spectra, step size = 30 μm). Integrated absorbances of OH bands were determined for the collection of spectra, choosing limits of 3705 cm^{-1} to 2880 cm^{-1} to include the broad OH band at 3400 cm^{-1} and sharp OH bands between 3595 cm^{-1} and 3379 cm^{-1} due to fluid inclusions and hydrogen defects, respectively, within quartz grains. Integrated absorbances of the 3600 cm^{-1} OH band of micas were determined between 3702 cm^{-1} to 3544 cm^{-1}, and this value, $\Delta_{OH\ musc}$ was subtracted from the

Solid Earth Discuss., doi:10.5194/se-2017-23, 2017
Manuscript under review for journal Solid Earth
Discussion started: 30 March 2017

first integrated absorbance (as illustrated in Fig. 3a) to represent the best measure of absorbance $\Delta_{OH\ qtz}$ of water and hydrogen defects of quartz grains.

These values were plotted spatially for Moine Thrust and Main Central Thrust samples, and contoured on common logarithm scales, to form high-resolution images (Figs. 6 - 9) of OH absorbance of quartz (converting to molar ppm, $OH/10^6Si$) and OH absorbance of micas ($\Delta_{OH\ musc}$ in cm^{-2}). In all cases, we superposed the contoured OH maps on optical micrographs to make sense of OH distributions in terms of fluid inclusions, defects, and micas, and their relationships to deformation and recrystallization microstructures. Images of the 3600 cm^{-1} mica OH absorbance were placed over plane light micrographs that highlight scattering (and sometimes color) due to micas, grain boundaries, and fluid inclusions, while images of OH absorbance due to fluid inclusions (principally the broad 3400 cm^{-1} band at large integrated absorbances) and lesser hydrogen defects of quartz were placed over cross-polarized light micrographs that emphasize undulatory extinction, deformation microstructures and recrystallization of quartz grains.

FTIR maps of OH of quartz grains show that water contents of deformed mylonites (Figs 6 - 8) are extremely heterogeneous when absorbance is dominated by the 3400 cm^{-1} band, with water contents that vary from 300 ppm to >10,000 ppm between neighboring grains and within grain interiors. This result helps explain the wide variations in water contents measured by conventional FTIR spectroscopy through a 100 μm aperture. OH contents of quartz grains of relatively dry mylonites (Fig. 9) are more nearly constant (50 - 150 ppm) when IR spectra are dominated by sharp OH bands of hydrogen point defects. FTIR maps of mylonite samples, constructed for the 3600 cm^{-1} OH absorbance, show that micas are heterogeneously distributed, with concentrations apparent at quartz grain boundaries in optical micrographs (Figs. 6 - 9) and finely dispersed micas within quartz grain interiors (Figs. 7, 8), some of which can be difficult to detect

Solid Earth Discuss., doi:10.5194/se-2017-23, 2017
Manuscript under review for journal Solid Earth
Discussion started: 30 March 2017

optically. We show these relationships in several contoured OH maps, focusing on different types of quartz grains and deformation microstructures.

While most quartz grains in Moine Thrust mylonites are highly deformed, some quartz grains remained nearly equant (globular grains or quartz augen with *c*-axes aligned perpendicular to foliation; Law et al., 1986), despite their high original OH contents in the form of fluid inclusions (Fig. 6). The lack of 3600 cm^{-1} OH absorbances within globular quartz grains indicate that finely dispersed micas in original relict quartz grains are absent, while large 3600 cm^{-1} OH absorbances at quartz grain extremities indicate that micas are localized at quartz grain boundaries (Fig. 6a, b). Broad band OH contents of quartz of >1000 ppm, thought to be sufficient for water weakening, are present in undeformed and deformed ribbon quartz grains (Fig. 6 c, d) with very large water contents (>10,000 ppm) marking a healed crack in the quartz augen, made up of a planar array of fluid inclusions. OH contents due to fluid inclusions are also very large at the globular augen quartz boundaries, coincident with high mica concentrations, and in some ribbon and recrystallized quartz grains. With a sample plate thickness of 56 μm, these maps represent OH absorbances within the interiors of larger quartz grains, while OH absorbances of fine micas and recrystallized quartz represent composite spectra of polycrystalline fault rock. However, we are confident that the quartz OH contents reflect fluid inclusions, even in these fine-grained regions, because of the simple spectral quality of muscovite (Fig. 3) in the Moine Thrust samples and our ability to distinguish between the 3400 cm^{-1} and 3600 cm^{-1} OH absorbances.

High-strain ribbon quartz grains in the Moine Thrust samples have large OH contents (>1000 ppm) comparable to those of water-weakened synthetic and milky quartz (samples SG-10 and SG-8, Figs. 7 and 8, respectively), with some reductions in OH at recrystallized margins of original grains. Micas, as imaged by the 3600 cm^{-1} OH absorbance (Fig. 7a, b), continue to be highly localized at the grain boundaries of deformed quartz grains, with a mixture of fine-grained mica

Solid Earth Discuss., doi:10.5194/se-2017-23, 2017
Manuscript under review for journal Solid Earth
Discussion started: 30 March 2017

and quartz grains providing evidence for some redistribution during recrystallization (Fig. 8a, b). The broad 3400 cm^{-1} OH absorbance in marginal recrystallized regions surrounding ribbon quartz grains are locally smaller than those of the original deformed quartz grains in some regions (Fig. 7 c, d) while broad OH absorbances of recrystallized quartz continue to be large where mica contents (as evidenced by the 3600 cm^{-1} band absorbance) are large (Fig. 8 c, d).

FTIR maps of coarse-grained Main Central Thrust mylonites yield spectral measurements of individual grains of quartz, muscovite and biotite, even for relatively thick IR plates and larger step sizes (Fig. 9). Small, sharp absorption bands of quartz grains yield OH contents of ~100 ppm, with only local regions of quartz with larger OH contents near contacts with coarse-grained muscovite and biotite grains. Quartz grain interiors generally lack the absorbance band at 3600 cm^{-1}; thus, there is no evidence for finely dispersed micas within these coarse-grained deformed (and recrystallized) quartz grains. Contours of integrated OH absorptions at 3400 cm^{-1} are considerably larger for coarse-grained micas and near their contacts with quartz grains. However, these bands cannot be attributed to fluid inclusions where they coincide with large 3600 cm^{-1} mica bands, given that muscovite and biotite grains in the Main Central Thrust samples exhibit complex secondary OH bands between 3311 and 2829 cm^{-1}.

5 Discussion

Our IR spectra collected from quartz-rich mylonites in the footwall to the Moine Thrust (Scottish Caledonides) and the hanging wall to the Main Central Thrust (Himalaya of NW India) using synchrotron IR radiation through a 10 μm aperture are comparable to IR spectra we collected for the same samples using a conventional FTIR-microscope system through a 100 μm aperture. The broad OH band and large water contents of the Moine Thrust mylonites deformed at 300 - 350°C are in line with previous FTIR studies of OH in quartz deformed under

Solid Earth Discuss., doi:10.5194/se-2017-23, 2017
Manuscript under review for journal Solid Earth
Discussion started: 30 March 2017

924 greenschist facies conditions. The sharp OH bands and low water contents of the
925 Main Central Thrust mylonites deformed at 570 - 610ºC are consistent with FTIR
926 studies of quartz in other shear zones deformed at amphibolite conditions (Han et
927 al., 2013; Kilian et al., 2016).
928 This study adds to an emerging impression that quartz tectonites deformed
929 at greenschist temperatures and natural strain rates are wet. Water contents of
930 quartz mylonites from other locations of the Moine Thrust deformed at greenschist
931 facies conditions vary from 1400 to 7500 ppm (Kronenberg and Wolf, 1990).
932 Water contents of deformed quartz across the Median Tectonic Line (Japan) vary
933 from 300 to 2500 ppm (Nakashima et al., 1995), depending on metamorphic grade
934 and shear displacement. Water contents of quartz deformed in granitic shear zones
935 and mylonites at greenschist conditions reach values of 1100 ppm and >10,000
936 ppm (Gleason and DeSisto, 2008; Kronenberg et al., 1990).
937 Our measurements of water in quartz grains in Main Central Thrust
938 mylonite samples build on the results of Nakashima et al. (1995), Han et al. (2013)
939 and Kilian et al. (2016), which suggest that quartz deformed at amphibolite
940 temperatures and natural strain rates may be relatively dry. Han et al. (2013)
941 report water contents of just 10 to 110 ppm for quartz grains of granitic mylonites
942 deformed at 400-500ºC within the Longmenshan tectonic zone (Sichuan, China).
943 Kilian et al. (2016) measured OH contents of just 20 to 100 ppm for quartz grains
944 of granitic mylonites deformed at upper amphibolite conditions (Truzzo meta-
945 granite, Central Alps, Italy), with IR spectra dominated by sharp OH bands due to
946 hydrogen point defects and no detectable broad band due to molecular water.
947 Significant water contents (1400-4400 ppm) have been observed for quartz
948 deformed at amphibolite conditions in mylonites of the El Pichao shear zone (NW
949 Argentina), though reductions in water content are evident with progressive
950 deformation (Finch et al., 2016). Fluid inclusions may be lost and intragranular
951 water contents reduced during high temperature deformation by a variety of
952 processes, from pipe diffusion (Bakker and Jansen, 1990, 1994; Hollister, 1990;

Solid Earth Discuss., doi:10.5194/se-2017-23, 2017
Manuscript under review for journal Solid Earth
Discussion started: 30 March 2017

Cordier et al., 1994; Mavrogenes and Bodnar, 1994) to recrystallization and grain boundary sweeping (Faleiros et al., 2010; Seaman et al., 2013; Finch et al., 2016; Kilian et al., 2016), and partial melting (Seaman et al., 2013).

5.1 Wide variations in OH content

All previous FTIR studies of quartz mylonites have revealed large variations in water content for different grains of the same fault rock, and FTIR mapping of OH (Seamon et al., 2013, and this study) has revealed significant variations within grains. Given that the broad OH band of quartz at 3400 cm^{-1} is isotropic, the grain-to-grain variations (at large water contents) are real, not owing to variations of dichroic OH band absorbance with quartz grain orientation for a uniform concentration of structurally incorporated hydrogen defects. Our FTIR measurements of quartz OH contents using a 10 μm aperture show that these variations depend on sampling volume, as observed by Kilian et al. (2016) who showed that broad OH band absorptions scale with size of the measurement area due to the inhomogeneous distributions of fluid inclusions.

The large and variable water contents of quartz mylonites are far above equilibrium solubilities (e.g., Paterson, 1986; Kronenberg et al., 1986; Cordier and Doukhan, 1989), and the variations in non-equilibrium OH contents probably reflect some part of the history of water migration during deformation. Images of contoured OH absorbances of the broad 3400 cm^{-1} band for quartz and the 3600 cm^{-1} bands of micas constructed for Moine Thrust and Main Central Thrust samples show relationships with optical deformation and recovery microstructures that suggest mechanisms by which water is incorporated in quartz grain interiors, how water becomes redistributed during deformation and recovery, and how water is lost from quartz grain interiors.

OH contours within relatively undeformed quartz augen of the Moine Thrust reveal planar zones of high water content that correspond to secondary

Solid Earth Discuss., doi:10.5194/se-2017-23, 2017
Manuscript under review for journal Solid Earth
Discussion started: 30 March 2017

fluid inclusions at healed microcracks (Fig. 6). We know little of this early brittle deformation, but these fluid inclusion arrays have microstructures similar to those generated during hydrothermal diffusional healing of cracks (Smith and Evans, 1984; Beeler and Hickman, 2015). As a result, early brittle deformation, infiltration of water along open cracks, and crack healing appears to be important to the early introduction of water to quartz grain interiors (Kronenberg et al., 1986, 1990, 2001; Diamond et al., 2010; Tarantola et al., 2010, 2012; Stünitz et al., in press).

OH contours in plastically deformed regions of Moine Thrust samples are complex and water contents appear to vary with strain patterns and recrystallization (Figs. 6 - 8). Clearly defined planar arrays of course fluid inclusions are absent from these regions, although the measured high water contents indicate redistribution of water within quartz grains rather than the loss of water. Processes of fluid inclusion decrepitation under deviatoric stresses have been studied experimentally (Diamond et al., 2010; Tarantola et al., 2010, 2012, Stünitz et al., in press), and they include simultaneous shrinkage of coarse (> 10 μm, optical-scale) inclusions, generation of dislocations at fluid inclusion walls, and formation of a new population of very fine (< 100 nm) fluid inclusions (visible only by transmission electron microscopy), which reside at dislocations and resemble water clusters and inclusions of deformed and heat-treated synthetic quartz (McLaren and Hobbs, 1972; White, 1973; Kirby and McCormick, 1979; Christie and Ord, 1980). The loss of coarse fluid inclusions and growth of fine inclusions requires diffusive transport, which may occur along interconnected and mobile dislocations (McLaren et al., 1983; 1989; Cordier et al., 1988, 1994; Bakker and Jansen, 1990, 1994; Hollister, 1990; Kronenberg et al., 1990, 2001; Tarontola et al., 2010, 2012; Stünitz et al., in press). Once formed, very fine fluid inclusions may also coarsen by pipe diffusion and processes documented by McLaren et al. (1983) and Cordier et al. (1988), leading to continuous changes in inclusion densities and size distributions.

Solid Earth Discuss., doi:10.5194/se-2017-23, 2017
Manuscript under review for journal Solid Earth
Discussion started: 30 March 2017

Some regions of recrystallized quartz grains in Moine Thrust samples appear to have somewhat lower OH contents than original ribbon quartz grains (Figs. 7), while highly recovered and recrystallized quartz grains in the Main Central Thrust samples have little or no detectable molecular water (Fig. 9). Reductions in intragranular water during dynamic recrystallization have been attributed to sweeping of fluid inclusions by mobile grain boundaries and losses of water from the fault rock by rapid grain boundary diffusion (Faleiros et al., 2010; Seaman et al., 2013; Finch et al., 2016; Kilian et al., 2016).

5.2 Limits on measurement volume

While synchrotron IR radiation has enabled spectral measurements through small (10x10 μm) apertured areas, we have not succeeded in measuring OH absorption bands for ultrathin samples when their interference fringes are larger than the absorption bands. Interference fringes due to internal reflections can be modeled (e.g., Clark and Moffatt, 1978; Pistorius and DeGrip, 2004; Konevskikh et al., 2015), but they become increasingly large as thickness of the doubly polished sample is reduced. For samples < 25 μm thick, we were unable to execute fringe corrections with sufficient confidence to measure OH spectra of individual, recrystallized quartz grains of the Moine Thrust.

The physical means by which we attempted to reduce interference fringes (rotating the sample within the IR beam, and changing numerical aperture of the IR objective) were also unsuccessful. However, interference fringes might be reduced in future studies by a number of other methods. Interference fringes could be eliminated if ultrathin samples are mounted on a substrate with a matching refractive index *n* (*personal communication*, Sina Marti). Such a substrate would need to be infrared-transparent, facilitate bonding between the sample and substrate (by low temperature melting or casting, to eliminate any residual air gaps between the sample and substrate), and lack OH bonds of its own. Alternatively,

Solid Earth Discuss., doi:10.5194/se-2017-23, 2017
Manuscript under review for journal Solid Earth
Discussion started: 30 March 2017

internal reflections could be reduced if thin samples are immersed in polychlorotrifluoroethylene oil (n = 1.41), which exhibits strong absorption bands at <2500 cm^{-1} but has only small bands (between 3600 and 3200 cm^{-1}) that might interfere with OH absorptions of the sample (*personal communication*, Jed Mosenfelder and George Rossman). Internal reflections could also be reduced if only one surface of the ultrathin IR plate is polished, leaving the other surface precision-ground for a given plate thickness t (as employed by Woodhead et al., 1991). Spectra measured with just one polished surface will suffer some signal loss and spectra will need to be corrected for background. Another method of reducing interference fringes that obscure OH absorption bands might be developed by focused ion beam (FIB) milling of one side of a doubly polished sample to eliminate reflections at that surface over the IR wavenumbers of interest (*personal communication*, Roy Christoffersen).

5.3 Water weakening in nature?

The water contents of Moine Thrust samples and other quartz mylonites deformed at greenschist conditions are large and variable, comparable to (and even larger than) those of wet varieties of synthetic and natural milky quartz (350-4000 ppm) that exhibit water weakening in laboratory studies (e.g., Griggs and Blacic, 1965; Kekulawala et al., 1978; Stünitz et al., in press). Highly deformed ribbon quartz grains, less deformed quartz augen, and recrystallized quartz grains of the Moine Thrust exhibit OH bands of similar character to those of quartzites deformed in laboratory experiments, a result that validates applications of wet quartzite rheologies to evaluate rates of dislocation creep in middle to upper crustal shear zones (e.g., Hirth et al., 2001; Behr and Platt 2011; Law, 2014).

In contrast, water contents of highly sheared and recrystallized quartz in the hanging wall of Main Central Thrust samples and other mylonites deformed at upper amphibolite conditions are much smaller than measured for wet varieties of

Solid Earth Discuss., doi:10.5194/se-2017-23, 2017
Manuscript under review for journal Solid Earth
Discussion started: 30 March 2017

quartz. The large shear strains accumulated over ~150-250 km of displacement along the Main Central Thrust (e.g., Srivastava and Mitra, 1994; Hodges, 2000; Mitra et al., 2010; Tobgay et al., 2012; Law et al., 2013) and quartz OH contents (50 - 150 ppm) far lower than required for water weakening challenge our understanding of dislocation creep and the role of water in deformation deep in the continental crust. With only few exceptions, IR spectra of Main Central Thrust samples have OH bands of the same character and size as dry natural quartz crystals, which are strong and have not been deformed by dislocation processes in laboratory experiments (e.g., Heard and Carter, 1968; Blacic, 1975; Blacic and Christie, 1984). Given sufficiently high temperatures, it is possible that quartz may deform at tectonic strain rates without critical hydrogen defects at dislocations and water weakening (Kilian et al., 2016). However, this implies that we have not measured flow laws for appropriately dry quartzites that we can apply to amphibolite conditions and natural strain rates. Alternatively, water may have been lost from quartz interiors following deformation. It is also possible that hydrogen defects that enhance dislocation motion at high temperatures and natural strain rates may be sourced from grain boundaries or micas, diffusing over longer distances than are possible at greenschist conditions or laboratory strain rates.

Spatial variations in OH content of quartz in natural shear zones, as mapped in this study, may provide key insights into the role of water weakening, and changes in water content during deformation and recrystallization. High resolution FTIR imaging of OH in Moine Thrust and Main Central Thrust samples show that water contents are increased, fluid inclusions are redistributed, and water contents are decreased during brittle deformation, plastic creep, recovery, and recrystallization. Changes in OH contents of quartz mylonites and the history of fluid migration during deformation may lead to changes in governing flow laws, non-steady rates of creep, and shifting zones of localized shear.

6 Conclusions

Solid Earth Discuss., doi:10.5194/se-2017-23, 2017
Manuscript under review for journal Solid Earth
Discussion started: 30 March 2017

1098

1099 The brightness of synchrotron IR radiation enables measurement of IR spectra for
1100 much smaller sampling volumes than is possible using conventional globar IR
1101 sources of FTIR instruments. In this study, we have used this improvement in
1102 signal to characterize and measure small OH absorption bands in quartz mylonites
1103 with an aperture size of 10 μm and to map water contents spatially. The ability to
1104 measure IR spectra for small, individual recrystallized grains by methods
1105 described in this study is limited by samples that must be > 40 μm thick to avoid
1106 internal reflections that lead to interference fringes that are larger than OH
1107 absorption bands. High-resolution images of OH in quartz mylonites, based on
1108 spectra collected through a 10 μm aperture as samples are translated under the
1109 beam, reveal large variations in OH content that correspond to the distributions of
1110 fluid inclusions and layer silicates, and to deformation and recrystallization
1111 microstructures. The OH contents of quartz in Moine Thrust mylonites deformed
1112 at greenschist conditions are comparable to wet quartzites deformed in the
1113 laboratory by processes of water weakening. By comparison, OH contents of
1114 quartz in Main Central Thrust mylonites deformed at upper amphibolite conditions
1115 are small, and molecular water, as required to deform quartz at experimental strain
1116 rates, is absent. What role water plays in deformation at these conditions is
1117 unclear, calling for further studies of water weakening in natural shear zones.
1118 High-resolution FTIR mapping of OH offers a new method of tracking changes in
1119 water content during deformation, recovery, and recrystallization.

1120

1121 *Acknowledgements*.

1122

1123 This study benefitted from helpful and enjoyable discussions with Kyle Ashley,
1124 Robert Tracy, Rüdiger Kilian, Sina Marti, Michael Stipp, Renee Heilbronner,
1125 Holger Stünitz, and Stephen Kirby. We thank Nicholas Davis for his outstanding
1126 work preparing beautifully thin, doubly polished IR plates; his skill, care, and

patience were invaluable to our work. We are indebted to Randy Smith of Brookhaven National Laboratory for sharing his expertise with OPUS imaging subroutines and teaching us how to compile and analyze integrated absorbances for multiple IR spectra collected over large scanned areas. Many thanks go to the leadership and staff of Brookhaven National Laboratory for operating the National Synchrotron Light Source NSLS I and awarding access to the U2A Beamline and Bruker Hyperion-2000 FTIR microscope. We thank the Consortium for Materials Properties Research in Earth Sciences COMPRES for their coordination of Earth science pursuits with other sciences done at NSLS. The National Science Foundation funded this work through a collaborative research grant awarded to the PIs at Virginia Tech (NSF EAR 1220345), Texas A&M University (NSF EAR 1220138), and Renssellaer Polytechnic Institute (transferred to Syracuse University, NSF EAR 1543627); their support is gratefully acknowledged.

References

Aines, R.D., and Rossman, G.R.: Water in minerals? a peak in the infrared, J. Geophys. Res., 89, 4059-4071, 1984.

Aines, R.D., Kirby, S.H., and Rossman, G.R.: Hydrogen speciation in synthetic quartz, Phys. Chem. Minerals, 11, 204-212, 1984.

Baeta, R.D., and Ashby, K.H.G.: Mechanical deformation of quartz I. constant strain-rate compression experiments, Phil. Mag., 22, 601-623, 1970.

Bai, Q., and Kohlstedt, D.L.: Effects of chemical environment on the solubility and incorporation mechanism for hydrogen in olivine, Phys. Chem. Minerals, 19, 460-471, 1996.

Bakker, R.J., and Jansen, J.B.H.: Preferential water leakage from fluid inclusions by means of mobile dislocations, Nature, 345, 58-60, 1990.

Bakker, R.J., and Jansen, J.B.H.: A mechanism for preferential H_2O leakage from fluid inclusions in quartz, based on TEM observations, Contrib. Mineral. Petrol., 116, 7-20, 1994.

1163 Beeler, N.M., and Hickman, S.H.: Direct measurement of asperity contact growth
1164 in quartz at hydrothermal conditions, J. Geophys. Res., 120, 3599-3616, doi:
1165 10.1002/2014JB011816, 2015.
1166
1167 Behr, W.M., and Platt, J.P.: A naturally constrained stress profile through the
1168 middle crust in an extensional terrane, Earth Planet. Sci. Lett., 303, 181-192,
1169 doi:10.1016/j.epsl.2010.11.044, 2011
1170
1171 Beran, A.: Infrared spectroscopy of micas, in: Micas: Crystal Chemistry and
1172 Metamorphic Petrology, Reviews in Mineralogy and Geochemistry, v. 46,
1173 edited by Mottana, A., Sassi, F.P., Thompson, J.B. Jr., Guggenheim, S.,
1174 Mineral. Soc. Amer., P.H. Ribbe Series Editor, Mineral. Soc. America,
1175 Washington, DC., Chap 7., 351-369, 2002.
1176
1177 Blacic, J.D.: Plastic deformation mechanisms in quartz: the effect of water,
1178 Tectonophysics, 27, 271-294, 1975.
1179
1180 Blacic, J.D.: Water diffusion in quartz at high pressure: tectonic implications,
1181 Geophys. Res. Letters, 8, 721-723, 1981.
1182
1183 Blacic, J.D., and Christie, J.M.: Plasticity and hydrolytic weakening of quartz
1184 single crystals, J. Geophys. Res., 89, 4223-4239, 1984.
1185
1186 Bonney, T.: Notes on some rocks collected by C. Callaway, Quarterly Journal of
1187 the Geological Society of London, 39, 414-422, 1883.
1188
1189 Butler, R.W.H.: The role of thrust tectonic models in understanding structural
1190 evolution in NW Scotland, in: Continental Tectonics and Mountain Building:
1191 The Legacy of Peach and Horne, edited by Law, R.D., Butler, R.W.H.,
1192 Holdsworth, R.E., Krabbendam, M., Strachan R.A., Geological Society,
1193 London, Special Publications, 335, 293-320, doi: 10.1144/SP335.14, 2010.
1194
1195 Carr, G.L., Smith, R.J., Mihaly, L., Zhang, H., Reitze, D.H., and Tanner, D.B.:
1196 High-resolution far-infrared spectroscopy at NSLS beamline U121R, Infrared
1197 Physics and Technology, 51, 404-406, doi: 10.1016/j.infrared.2007.12.034,
1198 2008.
1199
1200 Chernak, L.J., Hirth, G., Selverstone, J., and Tullis, J.: Effects of aqueous and
1201 carbonic fluids on the dislocation creep strength of quartz, J. Geophys. Res.,
1202 114, B04201, doi: 10.1029/2008JB005884, 2009.
1203
1204 Christie, J.M.: Mylonitic rocks of the Moine Thrust-zone in the Assynt region,
1205 north-west Scotland, Trans. Geol. Soc. Edinburgh, 18, 79-93, 1960.
1206

1207 Christie, J.M.: The Moine thrust zone in the Assynt region, northwest Scotland,
1208 University of California Publication Geological Science, 40, 345-440, 1963.
1209
1210 Christie, J.M., and Ord, A.: Flow stress from microstructures of mylonites:
1211 example and current assessment, J. Geophys. Res., 85, 6253-6262, 1980.
1212
1213 Christie, J.M., McIntyre, D.B., and Weiss, L.E.: Appendix to McIntyre, D.B.: The
1214 Moine thrust - its discovery, age and tectonic significance, Proceedings of the
1215 Geologists' Association, 65, 219-220, 1954.
1216
1217 Clark, F.R.S., and Moffatt, D.J.: The elimination of interference fringes from
1218 infrared spectra, Applied Spectroscopy, 32, 547-549, 1978.
1219
1220 Cordier, P. and Doukhan, J.-C.: Water solubility in quartz and its influence on
1221 ductility, Eur. J. Mineral., 1, 221-237, 1989.
1222
1223 Cordier, P., and Doukhan, J.-C.: Water speciation in quartz: a near infrared study,
1224 Amer. Min. 76, 361-369, 1991.
1225
1226 Cordier, P., Boulogne, B., and Doukhan, J.-C.: Water precipitation and diffusion
1227 in wet quartz and wet berlinite, $AlPO_4$, Bull. Mineral. 111, 113-137, 1988.
1228
1229 Cordier, P., Weil, J.A., Howarth, D.F., and Doukhan, J.-C.: Influence of the $(4H)_{Si}$
1230 defect on dislocation motion in crystalline quartz, Eur. J. Mineral., 6, 17-22,
1231 1994.
1232
1233 Dewey, J.F., Dalziel, I.W.D., Reavy, R.J., and Strachan, R.A.: The neoproterozoic
1234 to mid-Devonian evolution of Scotland: a review and unresolved issues,
1235 Scottish J. Geol., 51, 5-30, doi: 10.1144/sjg2014-007, 2015.
1236
1237 Diamond, L.W., Tarantola, A., and Stünitz, H.: Modification of fluid inclusions in
1238 quartz by deviatoric stress. II: experimentally induced changes in inclusion
1239 volume and composition, Contribs. Mineral. Petrol., 160, 845-864, doi:
1240 10.1007/s00410-010-0510-6, 2010.
1241
1242 Elliot, D., and Johnson, M.R.W.: The structural evolution of the northern part of
1243 the Moine thrust zone, Trans. Roy. Soc. Edinburgh, Earth Science, 71, 69-96,
1244 1990.
1245
1246 Faleiros, F.M., Campanha, G.A.C., Bello, R.M.S., and Fuzikawa, K.: Quartz
1247 recrystallization regimes, c-axis texture transitions and fluid inclusion
1248 reequilibration in a prograde greenschist to amphibolite facies mylonite zone
1249 (Ribeira Shear Zone, SE Brazil), Tectonophysics, 485, 193-214,
1250 doi:10.1016/j.tecto.2009.12.014.

Finch, M.A., Weinberg, R.F., and Hunter, N.J.R.: Water loss and the origin of thick ultramylonites, Geology, 44, 599-602, doi: 10.1130/G37972.1, 2016.

FitzGerald, J.D., Boland, J.N., McLaren, A.C., Ord, A., and Hobbs, B.E.: Microstructures in water-weakened single crystals of quartz, J. Geophys. Res., 96, 2139-2155, 1991.

Francsis, M.K.: Piezometry and Strain Rate Estimates along Mid-crustal Shear Zones, MS thesis, Virginia Tech, USA, http://scholar.lib.vt.edu/theses/available/etd-05032012-162325/, 2012.

Gerretsen, J., Paterson, M.S., and McLaren, A.C.: The uptake and solubility of water in quartz at elevated pressure and temperature, Phys. Chem. Min., 16, 334-342, 1989.

Gleason, G.C., and DeSisto, S.: A natural example of crystal-plastic deformation enhancing the incorporation of water into quartz, Tectonophysics, 446, 16-30, doi: 10.1016/j.tecto.2007.09.006, 2008.

Gleason, G.C., and Tullis, J.: A flow law for dislocation creep of quartz aggregates determined with the molten-salt cell, Tectonophysics, 247, 1-23, 1995.

Godin, L., Grujic, D., Law, R.D., and Searle, M.P.: Channel flow, ductile extrusion and exhumation in continental collision zones: an introduction, in: Channel Flow, Ductile Extrusion and Exhumation in Continental Collision Zones, edited by Law, R.D., Searle, M.P., Godin, L., Geological Society, London, Special Publications, 268, 1-23, doi: 10.1144/GSL.SP.2006.268.01.01, 2006.

Grasemann, B., Fritz, H., and Vannay J.C.: Quantitative kinematic flow analysis from the Main Central Thrust Zone (NW-Himalaya, India): implications for a decelerating strain path and the extrusion of orogenic wedges, J. Struct. Geol., 21, 837-853, doi: 10.1016/S0191-8141(99)00077-2, 1999.

Griffiths, P.R., and de Haseth, J.A.: Fourier Transform Infrared Spectroscopy, Wiley-Interscience, 529 p., 2007.

Griggs, D.T.: Hydrolytic weakening of quartz and other silicates, Geophys. J. Roy. Astr. Soc., 14, 19-31, 1967.

Griggs, D.T.: A model of hydrolytic weakening in quartz, J. Geophys. Res., 79, 1653-1661, 1974.

Griggs, D.T., and Blacic, J.D.: Quartz: anomalous weakness of synthetic crystals, Science, 147, 292-295, 1965.

Grujic, D., Casey, M., Davidson, C., Hollister, L.S., Kundig, K. Pavlis, T., and Schmid, S.: Ductile extrusion of the Higher Himalayan crystalline in Bhutan: evidence from quartz microfabrics, Tectonophysics, 260, 21-43, doi: 10.1016/0040-1951(96)00074-1, 1996.

Han, L., Zhou, Y.S., and He, C.R.: Water-enhanced plastic deformation in felsic rocks, Science Chinca-Earth Sciences, 56, 203-216, doi: 10.1007/s11430-012-4367-6, 2013.

Heard, H.C., and Carter, N.L.: Experimentally induced "natural" intragranular flow in quartz and quartzite, Amer. J. Sci., 266, 1-42, 1968.

Heilbronner, R., and Barrett, S.: Image Analysis in Earth Sciences, Microstructures and Textures of Earth Materials, Springer Verlag, Heidelberg, 520p., 2014.

Heller-Kallai, L., and Lapides, I.: Dehydroxylation of muscovite: study of quenched samples, Phys. Chem. Minerals, 42, 835-845, 2015.

Hirsch, P.B.: A mechanism for the effect of doping on dislocation mobility, J. Phys. Colloque C6 40, C6-117 - C6-121, 1979.

Hirth, G. and Tullis, J.: Dislocation creep regimes in quartz aggregates, J. Struct. Geol., 14, 145-159, 1992.

Hirth, G., Teyssier, C., and Dunlap, W.J.: An evaluation of quartzite flow laws based on comparisons between experimentally and naturally deformed rocks, Int. J. Earth Sciences, 90, 77-87, 2001.

Hobbs, B.E.: Recrystallization of single crystals of quartz, Tectonophysics, 6, 353-401, 1968.

Hobbs, B.E.: The influence of metamorphic environment upon the deformation of minerals, Tectonophysics, 78, 335-383, 1981.

Hodges, K.V.: Tectonics of the Himalaya and southern Tibet from two perspectives, Geol. Soc. Amer., Bull., 112, 324-350, doi:10.1130/0016-7606(2000)112<0324:TOTHAS>2.3.CO;2, 2000.

Hollister, L.S.: Enrichment of CO_2 in fluid inclusions in quartz by removal of H_2O during crystal-plastic deformation, J. Struct. Geol., 12, 895-901, 1990.

Holyoke, C.W. III, and Kronenberg, A.K.: Accurate differential stress measurement using the molten salt cell and solid salt assemblies in the Griggs apparatus with application to strength, piezometers and rheology, Tectonophysics, 494, 17-31, doi:10.1016/j.tecto.2010.08.001, 2010.

Holyoke, C.W. III, and Kronenberg, A.K.: Reversible water weakening of quartz, Earth and Planetary Science Letters, 374, 185-190, doi:10.1016/j.epsl.2013.05.039, 2013.

Jaoul, O., Tullis, J., and Kronenberg, A.K.: The effect of varying water contents on the creep behavior of Heavitree quartzite, J. Geophys. Res., 89, 4298-4312, 1984.

Johnson, M.R.W., Kelly, S.P., Oliver, G.J.H. and Winter, D.A.: Thermal effects and timing of thrusting n the Moine thrust zone, Journal of the Geological Society, London, 142, 863-874, 1985.

Kats, A.: Hydrogen in alpha quartz, Philips Research Reports, 17, 1-31, 133-195, 201-279, 1962.

Kekulawala, K.R.S.S., Paterson, M.S., and Boland, J.N.: Hydrolytic weakening in quartz, Tectonophysics, 46, T1-T6, 1978.

Kekulawala, K.R.S.S., Paterson, M.S., and Boland, J.N.: An experimental study of the role of water in quartz deformation, in: Mechanical Behavior of Crustal Rocks (The Handin Volume), edited by N.L. Carter, M. Friedman, J.M. Logan, and D.W. Stearns, Geophys. Monograph 24, Amer. Geophys. Union, Washington, DC, 49-60, 1981.

Kilian, R., Heilbronner, R., Holyoke C.W. III, Kronenberg, A.K., and Stünitz, H.: Dislocation creep of dry quartz, J. Geophys. Res., 121, 3278–3299, doi: 10.1002/2015JB012771, 2016.

Kirby, S.H., and McCormick, J.W.: Creep of hydrolytically weakened synthetic quartz crystals oriented to promote {2110}<0001> slip: a brief summary of work to date, Bull. Mineral., 102, 124-137, 1979.

Kohlstedt, D.L., Keppler, H., and Rubie, D.C.: Solubility of water in the α, β and γ phases of $(Mg,Fe)_2SiO_4$, Contrib. Mineral. Petrol., 123, 345-357, 1996.

Konevskikh, T., Ponossov, A., Blümel, R., Lukacs, R., and Kohler, A.: Fringes in FTIR spectroscopy revisted: understanding and modeling fringes in infrared spectroscopy of thin films, Analyst, 140, 3969-3980, doi:

10.1039/c4an02343a, 2015.

Kronenberg, A.K., and Tullis, J., Flow strengths of quartz aggregates: grain size and pressure effects due to hydrolytic weakening, J. Geophys. Res., 89, 4281-4297, 1984.

Kronenberg, A. K. and Wolf, G. H.: FTIR determinations of intragranular water content in quartz-bearing rocks: implications for hydrolytic weakening in the laboratory and within the Earth, Tectonophysics, 172, 255-271, 1990.

Kronenberg, A. K., Kirby, S. H., Aines, R. D. and Rossman, G. R.: Solubility and diffusional uptake of hydrogen in quartz at high water pressures: implications for hydrolytic weakening, J. Geophys. Res., 91, 12723-12744, 1986.

Kronenberg, A. K., Segall, P., and Wolf, G. H.: Hydrolytic weakening and penetrative deformation within a natural shear zone, in: The Brittle-Ductile Transition in Rocks (The Heard Volume), edited by A.G. Duba, W.B. Durham, J.W. Handin, and H.F. Wang, Geophys. Monograph 56, Amer. Geophys. Union, Washington, DC, 21-36, 1990.

Kronenberg, A.K., Lamb, W.M., Luo, Z., and Neal, L.A.: Redistribution of water during deformation of milky quartz, EOS Trans. AGU, 82, F1138, 2001.

Kruhl, J.H.: Prism- and basal-plane parallel subgrain boundaries in quartz: a microstructural geothermobarometer, J. Metamorphic Geol., 14, 581-589, 1996.

Kruhl, J.H.: Reply: Prism- and basal-plane parallel subgrain boundaries in quartz: a microstructural geothermobarometer, J. Metamorphic Geol, 16, 142-146, 1998.

Law, R.D.: Moine Thrust zone mylonites at the Stack of Glencoul: II - results of vorticity analyses and their tectonic significance, in: Continental Tectonics and Mountain Building: The Legacy of Peach and Horne, edited by Law, R.D., Butler, R.W.H., Holdsworth, R.E., Krabbendam, M., Strachan R.A., Geological Society, London, Special Publications, 335, 579-602, doi: 10.1144/SP335.23, 2010.

Law, R.D.: Deformation thermometry based on quartz c-axis fabrics and recrystallization microstructures: A review, J. Struct. Geol., 66, 129-161, doi: 10.1016/j.jsg.2014.05.023, 2014.

Law, R.D., Casey, M., and Knipe, R.J.: Kinematic and tectonic significance of microstructures and crystallographic fabrics within quartz mylonites from the

Assynt and Eriboll regions of the Moine thrust zone, NW Scotland, Trans. Roy. Soc. Edinburgh: Earth Sciences, 77, 99-125, 1986.

Law, R.D., and Johnson, M.R.W.: Microstructures and crystal fabrics of the Moine Thrust zone and Moine Nappe: history of research and changing tectonic interpretations, in: Continental Tectonics and Mountain Building: The Legacy of Peach and Horne, edited by Law, R.D., Butler, R.W.H., Holdsworth, R.E., Krabbendam, M., Strachan R.A., Geological Society, London, Special Publications, 335, 443-503, doi: 10.1144/SP335.21, 2010.

Law, R.D., Mainprice, D., Casey, M., Lloyd, G.E., Knipe, R.J., Cook, B., and Thigpen, J.R.: Moine Thrust zone mylonites at the Stack of Glencoul: 1 - microstructures, strain and influence of recrystallization on quartz crystal fabric development, in: Continental Tectonics and Mountain Building: The Legacy of Peach and Horne, edited by Law, R.D., Butler, R.W.H., Holdsworth, R.E., Krabbendam, M., Strachan R.A., Geological Society, London, Special Publications, 335, 543-577, doi: 10.1144/SP335.23, 2010.

Law, R.D., Searle, M.P., and Simpson, R.L.: Strain, deformation temperatures and vorticity of flow at the top of the Greater Himalayan Slab, Everest Massif, Tibet, J. Geological Society, 161, 305-320, doi: 10.1144/0016-764903-047, 2004.

Law, R.D., Stahr, D.W. III, Francsis, M.K., Ashley, K.T., Grasemann, B., Ahmad, T.: Deformation temperatures and flow vorticities near the base of the Greater Himalayan Series, Sutlej Valley and Shimla Klippe, NW India, J. Struct. Geol., 54, 21-53, 2013.

Linker, M.F., Kirby, S.H., Ord, A., and Christie, J.M.: Effects of compression direction on the plasticity and rheology of hydrolytically weakened synthetic quartz crystals at atmospheric pressure, J. Geophys. Res., 89, 4241-4255, 1984.

Lister, G.S.: Crossed-girdle *c*-axis fabrics in quartzites plastically deformed by plane strain and progressive simple shear, Tectonophysics, 39, 51-54, doi: 10.1016/0040-1951(77)90087-7, 1977.

Lobo, R.P.S.M., LaVeigne, J.D., Reitze, D.H., Tanner, D.B., and Carr, R.L.: Performance of new infrared beamline U121R at the National Synchrotron Light Source, Review of Scientific Instruments, 70, 2899-2904, doi: 10.1063/1.1149846, 1999.

Ma M. Liu, W., Chen, Z., Liu, Z., and Li B.: Compression and structure of brucite to 31 GPa from synchrotron X-ray diffraction and infrared spectroscopy

studies, Amer. Min., 98, 33-40, doi: 10.2138/am.2013.4117, 2013.

Mackwell, S.J., and Kohlstedt, D.L.: Diffusion of hydrogen in olivine - implications for water in the mantle, J. Geophys. Res., 95, 5079-5088.

Mavrogenes, J.A., and Bodnar, R.J.: Hydrogen movement into and out of fluid inclusions in quartz: experimental evidence and geological implications, Geochim. Cosmochim. Acta, 58, 141-148, 1994.

McLaren, A.D., and Hobbs, B.E.: Transmission electron microscope investigations of some naturally deformed quartzites, in: Flow and Fracture of Rocks, edited by Heard, H.C., Borg, I.Y., Carter, N.L., and Raleigh, C.B., Geophys. Monograph 16, 55-66, Amer. Geophys. Union, Washington, D.C., 1972.

McLaren, A.C., Cook, R.F., Hyde, S.T., and Tobin, R.C.: The mechanisms of the formation and growth of water bubbles and associated dislocation loops in synthetic quartz, Phys. Chem. Min., 9, 79-94, 1983.

McLaren, A.C., FitzGerald, J.D., and Gerretsen, J.: Dislocation nucleation and multiplication in synthetic quartz: relevance to water weakening, Phys. Chem. Minerals, 16, 465-482.

Mitra, G., Bhattacharyya, K., and Mukul, M.: The lesser Himalayan duplex in Sikkim: implications for variations in Himalayan shortening, J. Geol. Soc. India, 75, 289-301, 2010.

Muto, J., Hirth, G., Heilbronner, R., and Tullis, J.: Plastic anisotropy and fabric evolution in sheared and recrystallized quartz single crystals, J. Geophys. Res., 116, 1-18, 2011.

Nakashima, S., Matayoshi, H., Yuko, T., Michibayashi, K., Masuda T., Kuroki, N., Yamagishi, H., Ito, Y., and Nakamura, A.: Infrared microspectroscopy analysis of water distribution in deformed and metamorphosed rocks, Tectonophysics, 245, 263-276, doi: 10.1016/0040-195(94)00239-6, 1995.

Ord, A., and Christie, J.M.: Flow stresses from microstructures in mylonitic quartzites of the Moine Thrust zone, Assynt area, Scotland, J. Struct. Geol., 6, 639-654, 1984.

Powell, R., and Holland, T.: Optimal geothermometry and geobarometry, Amer. Mineral., 79, 120-133, 1994.

Paterson, M.S.: The thermodynamics of water in quartz, Phys. Chem. Minerals,

13, 245-255, 1986.

Paterson, M.S.: The interaction of water with quartz and its influence in dislocation flow - an overview, in: Rheology of Solids and of the Earth, edited by S.-I. Karato and M. Toriumi, Oxford University Press, Oxford, 107-142, 1989.

Peach, B.N., Horne, J., Gunn, W., Clough, C.T., and Hinxman, L.W., The geological structure of the north-west Highlands of Scotland, Memoir Geological Survey Great Britain, HMSO, Glasgow, 1907.

Pistorius, A.M.A., and DeGrip, W.J.: Deconvolution as a tool to remove fringes from an FT-IR spectrum, Vibrational Spectroscopy, 36, 89-95, doi: 10.1016/j.vibspec.2004.04.001, 2004.

Post, A.D., Tullis, J., and Yund, R.A.: Effects of chemical environment on dislocation creep of quartzite, J. Geophys. Res., 101, 22143-22155, 1996.

Prieto, A.C., Dubessy, J., and Cathelineau, M.: Structure-composition relationships in trioctahedral chlorites: a vibrational spectroscopy study, Clays and Clay Minerals, 39, 531-539, 1991.

Seaman, S.J., Williams, M.L., Jercinovic, M.J., Koteas, G.C., and Brown, L.B.: Water in nominally anhydrous minerals: implications for partial melting and strain localization in the lower crust, Geology, 41, 1051-1054, doi: 10.1130/G34435.1, 2013.

Searle, M.P., Simpson, R.L., Law, R.D., Parrish, R.R., and Waters, D.J.: The structural geometry, metamorphic and magmatic evolution of the Everest massif, High Himalaya of Nepal-South Tibet, J Geological Society, 160, 345-366, doi: 10.1144/0016-764902-126, 2003.

Searle, M.P., Law, R.D., Godin, L., Larson, K.P., Streule, M.J., Cottle, J.M., and Jessup, M.J.: Defining the Himalayan Main Central Thrust in Nepal, J. Geological Society, London, 165, 523-534, 2008.

Smith, D.L., and Evans, B.: Diffusional crack healing in quartz, J. Geophys. Res., 89, 4125-4135, 1984.

Snoke, A.W., Tullis, J., and Todd, V.R.: Fault-related Rocks, A Photographic Atlas, Princeton University Press, Princeton, 617p., 1998.

Srivastava, P., and Mitra, G.: Thrust geometries and deep structure of the outer and lesser Himalaya, Kumaon and Garhwal (India): implications for evolution

of the Himalayan fold-and-thrust belt, Tectonics, 13, 89-109,1994.

Stahr, D.W.: Kinematic Evolution, Metamorphism and Exhumation of the Himalayan Series, Sutlej River and Zanskar Regions of NW India. PhD thesis, Virginia Tech, USA, https://vtechworks.lib.vt.edu/handle/10919/23081, 2013.

Stipp, M., Stünitz, H., Heilbronner, R., and Schmid, S.M.: The eastern Tonale fault zone: a 'natural laboratory' for crystal plastic deformation of quartz over a temperature range from 250 to 700 degrees C, J. Struct. Geol., 24, 1861-1884, doi: 10.1016/S0191-8141(02)00035-4, 2002

Stipp, M., and Tullis, J.: The recrystallized grain size piezometer for quartz, Geophys. Res. Letters, 30, 2088, doi: 10.1029/2003GL018444, 2003.

Stipp, M., Tullis, J., and Behrens, A.: Effect of water on the dislocation creep microstructure and flow stress of quartz and implications for the recrystallized grain size piezometer, J. Geophys. Res., 111, 201-220, 2006.

Stipp, M., Tullis, J., Scherwarth, M., and Behrmann, J.H.: A new perspective on paleopiezometry: Dynamically recrystallized grain size distributions indicate mechanism changes, Geology, 38, 759-762, doi: 10.1130/G31162.1, 2010.

Stuart, B.H., George, B., and McIntyre, P.: Modern Infrared Spectroscopy, J. Wiley and Sons, 200 p., 1996.

Stünitz, H., Thust, A., Heilbronner, R., Behrens, H., Kilian, R., Tarantola, A., and FitzGerald, J.D.: Water redistribution in experimentally deformed natural milky quartz single crystals - implications for H_2O-weakening processes, J. Geophys. Res., in press.

Tarantola, A., Diamond, L.W., and Stünitz, H.: Modification of fluid inclusions in quartz by deviatoric stress I: experimentally induced changes in inclusion shapes and microstructures, Contrib. Mineral. Petrol., 160, 825-843, doi: 10.1007/s00410-010-0509-z, 2010.

Tarantola, A., Diamond, L.W., Stünitz, H., Thust, A., and Pec, M.: Modification of fluid inclusions in quartz by deviatoric stress. III: influence of principal stresses on inclusion density and orientation, Contribs. Mineral. Petrol., 164, 537-550, doi: 10.1007/s00410-012-0749-1, 2012.

Thigpen, J.R., Law, R.D., Lloyd, G.E., and Brown, S.J.: Deformation temperatures, vorticity of flow, and strain in the Moine thrust zone and Moine nappe: Reassessing the tectonic evolution of the Scandian foreland-hinterland

transition zone, J. Struct. Geol., 32, 920-940, doi: 10.1016/j.jsg.2010.05.001, 2010.

Thigpen, J.R., Law, R.D., Loehn, C.L., Strachen, R.A., Tracy, R.J., Lloyd, G.E., Roth, B.L., and Brown, S.J.: Thermal structure and tectonic evolution of the Scandian orogenic wedge, Scottish Caledonides: integrating geothermometry, deformation temperatures and conceptual kinematic-thermal models, J. Metamorph. Geol., 31, 813-842, doi: 10.1111/jmg.12046, 2013

Thomas, S.-M., Koch-Müller, M., Reichert, P., Rhede, D., Thomas, R., Wirth, R., and Matsyuk, S.: IR calibrations for water determination in olivine, r-GeO_2, and SiO_2 polymorphs, Phys. Chem. Minerals, 36, 489-509, doi: 10.1007/s00269-009-0295-1, 2009.

Tobgay, T., McQuarrie, N., Long, S., Kohn, M.J., and Corrie, S.L.: The age and rate of displacement along the Main Central Thrust in the western Bhutan Himalaya, Earth Planet. Sci. Letts., 319-320, 146-158, doi: 10.1016/j.epsl.2011.12.005, 2012.

Tokiwai, K., and Nakashima, S.: Integral molar absorptivities of OH in muscovite at 20 to 650ºC by in-situ high-temperature IR microspectroscopy, Amer. Min. 95, 1052-1059, 2010a.

Tokiwai, K., and Nakashima, S.: Dehydration kinetics of muscovite by in situ infrared microspectroscopy, Phys. Chem. Minerals, 37, 91-101, 2010b.

Tullis, J.: Deformation of feldspars, Chap. 13, in: Feldspar Mineralogy, Second Edition, edited by P.H. Ribbe, Reviews in Mineralogy, v.2, Min. Soc. Amer., Washington DC, 297-324, 1983.

Tullis, J., and Yund, R.A.: Experimental deformation of dry Westerly granite, J. Geophys. Res., 82, 5705-5718, 1977.

Tullis, J., and Yund, R.A.: Hydrolytic weakening of experimentally deformed Westerly granite and Hale albite rock, J. Struct. Geol., 2, 439-451, 1980.

Tullis, J., and Yund, R.A.: Hydrolytic weakening of quartz aggregates: the effects of water and pressure on recovery, Geophys. Res. Letters, 16, 1343-1346, 1989.

Vannay, J.C., and Grasemann, B.: Inverted metamorphism in the High Himalaya of Himachal Pradesh (NW India): phase equilibria versus thermobarometry, Schweizerische Mineralogische und Petrographische Mitteilungen, 78, 107-132, 1998

Solid Earth Discuss., doi:10.5194/se-2017-23, 2017
Manuscript under review for journal Solid Earth
Discussion started: 30 March 2017

Weathers, M.S., Bird, J.M., Cooper, R.F., and Kohlstedt, D.L.: Differential stress determined from deformation-induced microstructures of the Moine thrust zone, J. Geophys. Res., 84, 7495-7509, 1979.

White, S.: Dislocations and bubbles in vein quartz, Nature Phys. Sci., 243, 11-14, 1973.

Woodhead, J.A., Rossman, G.R., and Thomas, A.P.: Hydrous species in zircon, Amer. Min., 76, 1533-1546, 1991.

Zhang, M., Tarantino, S.C., Su, W., Lou, X. Ren, X., Salje, E.K.H., Carpenter, M.A., and Redfern, S.A.T.: Optical phonons, OH vibrations, and structural modifications of phlogopite at high temperatures: an in-situ infrared spectroscopic study, Amer. Min., 101, 1873-1883, 2016.

Table Captions

Table 1. Structural distances of samples below the Moine Thrust at the Stack of Glencoul (Law et al., 1986, 2010) and above the Main Central Thrust on the NW and Eastern Sutlej transects (Law et al., 2013). Deformation temperatures estimated by Law et al. (2013) using the Kruhl (1998) quartz *c*-axis fabric opening angle thermometer, and temperatures and pressures of metamorphism estimated by Stahr (2013) using THERMOCALC multi-equilibria thermometry (Powell and Holland 1994) are indicated.

Figure Captions

Figure 1. Doubly polished IR plates of Moine Thrust mylonites prepared perpendicular to foliation and parallel to lineation. (a) Low magnification image of large IR plate prepared from Stack of Glencoul sample SG-10 (unpolarized light imaged in high resolution Nikon slide scanner), with a mean thickness t = 120 μm. (b) Same IR plate of SG-10 shown in (a) but with crossed-polarized light. The Moine Thrust transport direction is shown in the plane of the IR plate

Solid Earth Discuss., doi:10.5194/se-2017-23, 2017
Manuscript under review for journal Solid Earth
Discussion started: 30 March 2017

(top to the left, in the geographic WNW direction). (c) Higher magnification optical micrograph of large IR plate of sample SG-10, with crossed polarized light and local plate thickness (117 μm) determined from IR interference fringes. (d) Optical micrograph of Stack of Glencoul sample SG-7 in crossed-polarized light (normal 30 μm section thickness), illustrating deformation and recover microstructures with higher resolution than in thick IR plates, with undulatory extinction in ribbon quartz grains, fine recrystallized grains and aligned muscovite grains localized at quartz grain boundaries. (e) Low magnification image of ultrathin IR plate of Stack of Glencoul sample SG-7-5 (crossed-polarized light) mounted on a copper TEM slot ring (t = 4-8 μm, based on IR interference fringes). (f) Higher magnification optical micrograph of the same IR plate SG-7-5 (crossed-polarized light) as shown in (e) with deformation and recrystallization microstructures shown more clearly than in normal 30 μm thin section.

Figure 2. IR spectra of quartz grains in mylonites from the Moine Thrust (Stack of Glencoul) and the Main Central Thrust (Sutlej Valley) using conventional FTIR with globar IR source through a 100 μm aperture. (a) Absorbance spectra of quartz grains of Moine Thrust IR plate SG-10 (shown in Fig. 1, t = 120 μm) showing broad OH band at 3400 cm^{-1} associated with fluid inclusions in milky quartz. (b) Absorption spectra of Moine Thrust quartz grains of the same IR plate (SG-10) showing the same broad OH band due to fluid inclusions in addition to an OH absorption band (or shoulder) at 3600 cm^{-1} due to mica inclusions. (c) Absorbance spectra of quartz grains of Main Central Thrust IR plates S09-30 (t = 121 μm), S09-35 (t = 74 μm), and S09-58 (t = 145 μm), with many grains showing small sharp OH absorption bands at 3595, 3482, 3431, 3408, and 3379 cm^{-1} due to hydrogen point defects, and less common grains with a large broad absorption band at 3400 cm^{-1}. (d) Absorption spectra of quartz grains of Main Central Thrust sample S09-30 (t = 121 μm) with a prominent OH band at 3600 cm^{-1} due to mica inclusions and smaller OH bands at lower wavenumbers. Absorbance values

Solid Earth Discuss., doi:10.5194/se-2017-23, 2017
Manuscript under review for journal Solid Earth
Discussion started: 30 March 2017

plotted vertically are normalized to represent their values for a uniform sample thickness of 1 mm.

Figure 3. OH absorption bands due to fluid inclusions and hydrogen defects in quartz grains and those due to mica inclusions. (a) Integrated absorbances of OH bands at 3400 cm^{-1} (due to fluid inclusions) and 3595 to 3379 cm^{-1} (due to hydrogen interstitials) of quartz grains ($\Delta_{OH\ qtz}$ in cm^{-2}) can be separated from the integrated absorbance of the 3600 cm^{-1} OH band of mica inclusions ($\Delta_{OH\ mica}$), depending on the IR absorption spectra of the micas. The integrated absorbance Δ of the 3600 cm^{-1} OH band of micas can be determined over 3702 cm^{-1} to 3544 cm^{-1}, fitting a straight line between these values. In order to evaluate the remaining OH absorbance of the spectrum, the value of Δ determined for the 3600 cm^{-1} band is deducted from value from the integrated absorbance Δ due to all OH absorptions over 3705 cm^{-1} to 2880 cm^{-1}, again fitting the background by a straight line. This procedure works well to distinguish OH absorbances due to muscovite inclusions ($\Delta_{OH\ musc}$) from those of fluid inclusions and hydrogen defects of Moine Thrust quartz grains ($\Delta_{OH\ qtz}$ determined for SG-10, Grain 2, t = 120 μm), given that (b) the absorption spectrum of muscovite grains in Moine Thrust samples is very simple, with one prominent OH absorption band at 3620 cm^{-1} (t = 8 μm, absorbance normalized to t = 0.1 mm). OH absorption spectra of (c) muscovite and (d) biotite grains of Main Central Thrust mylonites (S09-63, t = 155 um) are more complex than displayed by muscovite grains of the Moine Thrust. The prominent OH band of muscovite grains in Main Central Thrust samples appears at 3638 cm^{-1} with smaller OH bands at 3815, 3311, 3146, and 3035 cm^{-1}. The primary OH band of biotite grains in Main Central Thrust samples appears at 3614 cm^{-1} (with shoulders at 3674 and 3561 cm^{-1}) and secondary OH bands at 3258, 3043, and 2829 cm^{-1}. The OH bands of all micas at ~3600 cm^{-1} are highly anisotropic; absorbances at ~3600 cm^{-1} for muscovite grains measured in polarized IR radiation are maximized when the vibration direction E is parallel to

Solid Earth Discuss., doi:10.5194/se-2017-23, 2017
Manuscript under review for journal Solid Earth
Discussion started: 30 March 2017

the basal (001) plane, while principal OH absorbances for biotite grains are maximized when E is perpendicular to (001). However, secondary OH bands of muscovite and biotite grains of the Main Central Thrust show significant variations from the dichroism displayed by the primary OH bands of each of these micas. The complex nature of these secondary OH bands presents significant difficulties in separating OH absorptions of quartz grains due to molecular water and hydrogen defects and those due to mica inclusions dispersed within quartz grains. All absorption spectra shown here were measured using unpolarized IR radiation with a conventional FTIR spectrometer and a 100 μm aperture. Absorbances for all spectra but (b) are normalized to a uniform thickness t of 1 mm.

Figure 4. IR spectra of quartz grains in Moine Thrust mylonite samples (Stack of Glencoul), measured with synchrotron-FTIR system using a 10 μm aperture with varying IR plate thicknesses (a) t = 113 μm (BSG 10, local plate thickness determined from interference fringes), (b) t = 13 μm (SG-10.2t), and (c) t = 6.5 μm (BSG 7.3, sample plate SG-7-1). For doubly polished sample plates of ~100 μm, IR spectra measured using the coupled synchrotron-FTIR spectrometer system through a 10 μm aperture are similar to those measured using a conventional FTIR spectrometer through a 100 μm aperture. (a) IR spectra of Moine Thrust sample (SG-10) show OH absorption bands of similar character at the same wavenumbers for a 10 μm aperture as OH bands measured through a larger (100 μm) aperture, including a large broad absorption band at 3400 cm^{-1} due to dispersed fluid inclusions (both BSG 10.1 and BSG 10.3) and a sharper band at 3600 cm^{-1} due to mica inclusions (shown by BSG 10.3). Interference fringes in samples ~100 μm thick are apparent, allowing determination of local IR plate thickness, but they do not obscure the OH absorption bands. (b) Interference fringes for samples < 25 μm thick are large, and make detection of small OH absorption bands difficult. The only detectable absorbance bands in sample SG-

Solid Earth Discuss., doi:10.5194/se-2017-23, 2017
Manuscript under review for journal Solid Earth
Discussion started: 30 March 2017

1767 10.2t (t = 13 μm) are due to strong primary Si-O vibrations (at $\upsilon < 2200$ cm^{-1});
1768 OH absorption bands cannot be resolved. (c) Interference fringes are very large
1769 for thin IR plates (t = 6.5 μm; SG-7-1); OH absorption bands are not observed,
1770 even after attempts to model them and remove fringes numerically. All
1771 absorbance values (and apparent absorbance values of interference fringes
1772 exhibited by SG-7) are normalized to a uniform sample thickness of 1 mm.
1773
1774 **Figure 5.** Ultrathin IR plates (t = 4-8 μm) exhibit deformation microstructures in
1775 crossed-polarized light with greater clarity than those of conventional thin sections
1776 (t = 30 μm). (a) Deformed ribbon quartz grains of Moine Thrust sample SG-7-6 (t
1777 = 6-8 μm) show distinct subgrains with sharply defined subgrain walls, while
1778 extinction in conventional thin sections of ribbon quartz is smoothly varying and
1779 subgrain boundaries are difficult to detect. Finely recrystallized quartz grains at
1780 sutured grain boundaries are smaller than subgrains within large deformed quartz
1781 grains. (b) Less deformed quartz porphyroclast of Moine Thrust sample SG-7-5 (t
1782 = 5-6 μm) with internal subgrains, and surrounding recrystallized quartz grains of
1783 similar dimensions to those of internal subgrains.
1784
1785 **Figure 6.** OH absorbance maps of Moine Thrust sample SG-7 constructed from
1786 900 IR spectra (SG-7t-1map, 30 x 30 steps, 10 μm/step) for a doubly polished
1787 plate prepared (56 μm thick) perpendicular to foliation and parallel to the transport
1788 direction (lineation horizontal in all panels). (a) Plane-polarized micrograph of IR
1789 plate SG-7t showing nearly equant globular augen quartz grain surrounded by
1790 highly deformed ribbon and recrystallized quartz grains. Light scattering is mostly
1791 due to micas and fluid inclusions. Outlined box is the region imaged by integrated
1792 IR absorbances. (b) The same plane-polarized light micrograph as in (a) with
1793 superposed map of OH absorbance of the 3600 cm^{-1} band due to micas (OH of
1794 micas given in integrated area cm^{-2}). Contours are given in $\log_{10}(\Delta$ in cm$^{-2})$ for the
1795 integrated absorbance of the ~3600 cm^{-1} OH band. (c) Cross-polarized light

Solid Earth Discuss., doi:10.5194/se-2017-23, 2017
Manuscript under review for journal Solid Earth
Discussion started: 30 March 2017

micrograph of the same region of IR plate SG-7t as shown in (a), with subtle undulatory extinction of ribbon quartz shown in white and first-order interference colors. (d) The same cross-polarized light micrograph as in (c) with superposed map of OH absorbance of the broad 3400 cm^{-1} band due to molecular water in fluid inclusions (and smaller OH bands due to hydrogen defects) of quartz grains (OH of quartz in molar ppm, $OH/10^6$ Si). Contours given in $\log_{10}$ (ppm) for integrated absorbance of the broad 3400 cm^{-1} OH band (and lesser sharp OH bands) of quartz. OH contents of quartz and those associated with micas are contoured in color with blue (and cool colors) corresponding to large water (OH) contents, and red (and warm colors) corresponding to low water (OH) contents.

Figure 7. OH absorbance maps of Moine Thrust sample SG-10 constructed from 3600 IR spectra (SG-10-XY2, 60 x 60 steps, 10 μm/step) for a doubly polished plate prepared (117 μm thick) perpendicular to foliation and parallel to the transport direction (lineation horizontal in all panels). (a) Plane-polarized micrograph of IR plate SG-10-2 showing deformed ribbon quartz grains surrounded by recrystallized quartz grains. Light scattering is mostly due to micas and fluid inclusions. Outlined box is the region imaged by integrated IR absorbances. (b) The same plane-polarized light micrograph as in (a) with superposed map of OH absorbance of the 3600 cm^{-1} band due to micas (OH of micas given in integrated area Δ cm^{-2} and contoured as $\log_{10} \Delta$). (c) Cross-polarized light micrograph of the same region of IR plate SG-10-2 as shown in (a), with undulatory extinction of deformed ribbon quartz grains, incipient recrystallized grains at quartz ribbon margins, and recrystallized matrix grains shown by first-order interference colors. (d) The same cross-polarized light micrograph as in (c) with superposed map of OH absorbance of the broad 3400 cm^{-1} band due to molecular water in fluid inclusions (and smaller OH bands due to hydrogen defects) of quartz grains (OH of quartz in molar ppm, $OH/10^6$ Si and contoured as $\log_{10}$ OH). OH contents of quartz and those associated with micas

Solid Earth Discuss., doi:10.5194/se-2017-23, 2017
Manuscript under review for journal Solid Earth
Discussion started: 30 March 2017

1825 are contoured in color with blue (and cool colors) corresponding to large water
1826 (OH) contents, and red (and warm colors) corresponding to low water (OH)
1827 contents.
1828
1829 **Figure 8.** OH absorbance maps of Moine Thrust sample SG-8 constructed from
1830 1800 IR spectra (SG-8t-map1, 30 x 60 steps, 10 μm/step) for a doubly polished
1831 plate prepared (73 μm thick) perpendicular to foliation and parallel to the transport
1832 direction (lineation horizontal in all panels). (a) Plane-polarized micrograph of IR
1833 plate SG-8t showing deformed ribbon quartz grains and regions of finely dispersed
1834 mica and recrystallized quartz grains. Light scattering is mostly due to micas,
1835 fluid inclusions, and grain boundaries. Outlined box is the region imaged by
1836 integrated IR absorbances. (b) The same plane-polarized light micrograph as in
1837 (a) with superposed map of OH absorbance of the 3600 cm^{-1} band due to micas
1838 (OH of micas given in integrated area Δ cm^{-2} and contoured as $\log_{10} \Delta$). (c) Cross-
1839 polarized light micrograph of the same region of IR plate SG-8t as shown in (a),
1840 with undulatory extinction of deformed ribbon quartz grains and regions of
1841 recrystallized grains shown by first-order interference colors. (d) The same cross-
1842 polarized light micrograph as in (c) with superposed map of OH absorbance of the
1843 broad 3400 cm^{-1} band due to molecular water in fluid inclusions (and smaller OH
1844 bands due to hydrogen defects) of quartz grains (OH of quartz in molar ppm,
1845 $OH/10^6$ Si and contoured as $\log_{10}$ OH). OH contents of quartz and those
1846 associated with micas are contoured in color with blue (and cool colors)
1847 corresponding to large water (OH) contents, and red (and warm colors)
1848 corresponding to low water (OH) contents.
1849
1850 **Figure 9.** OH absorbance maps of Main Central Thrust sample S09-63
1851 constructed from 1200 IR spectra (S09-63-map1, 30 x 40 steps, 50 μm/step) for a
1852 doubly polished plate prepared (155 μm thick) perpendicular to foliation and
1853 parallel to the transport direction (lineation horizontal in all panels). (a) Plane-

Solid Earth Discuss., doi:10.5194/se-2017-23, 2017
Manuscript under review for journal Solid Earth
Discussion started: 30 March 2017

polarized micrograph of IR plate S-09-63 showing coarse, clear quartz grains, and coarse muscovite and biotite grains with readily distinguishable color and pleochroism. Scattering of light is primarily due to grain boundaries, with little evidence for dense fluid inclusions or finely dispersed micas. Outlined box is the region imaged by integrated IR absorbances. (b) The same plane-polarized light micrograph as in (a) with superposed map of OH absorbance of the 3600 cm^{-1} band due to micas (OH of micas given in integrated area Δ cm^{-2} and contoured as $\log_{10} \Delta$). (c) Cross-polarized light micrograph of the same region of IR plate SG-09-63 as shown in (a), with high-temperature deformation and recovery microstructures (in higher order interference colors) that are characterized by subtle (to absent) undulatory extinction of quartz, subgrain walls, and coarse recrystallized grains. (d) The same cross-polarized light micrograph as in (c) with superposed map of OH absorbance over 3705 and 2880 cm^{-1} to capture the broad and sharp bands of quartz, deducting the large 3600 cm^{-1} band of micas, but including smaller OH bands of micas between 3311 and 2920 cm^{-1}. Contours in this absorbance can only be attributed unambiguously to fluid inclusions and hydrogen defects in quartz where micas (and their 3600 cm^{-1} absorbances) are absent. OH contents of quartz and those associated with micas are contoured in color with blue (and cool colors) corresponding to large water (OH) contents, and red (and warm colors) corresponding to low water (OH) contents.

Solid Earth Discuss., doi:10.5194/se-2017-23, 2017
Manuscript under review for journal Solid Earth
Discussion started: 30 March 2017

Moine Thrust - Stack of Glencoul mylonitic quartzites

Sample	Distance below MT
SG.7	2.5 m
SG.8	2.9 m
SG.10	4.6 m

Main Central Thrust - NW Sutlej transect orthogneisses

Sample	Distance above MCT	T
S09-30	~ 750 m	~ 600°C[1]
S09-35	75 m	~ 540°C[1]

Main Central Thrust - Eastern Sutlej transect paragneisses

Sample	Distance above MCT	T	P
S09-58	~ 4,500 m	735°C[2]	900 MPa[2]
S09-63	~1500 m	675°C[2]	850 MPa[2]
S09-71B	25 m	610°C[1]	

[1]Deformation temperature estimated from quartz *c*-axis fabric opening angle (Law et al. 2013).

[2]Temperature and pressure of metamorphism estimated from THERMOCALC multi-equilibra thermobarometry (Stahr 2013, p. 67; Law et al., 2013).

Solid Earth Discuss., doi:10.5194/se-2017-23, 2017
Manuscript under review for journal Solid Earth
Discussion started: 30 March 2017

Fig. 1a

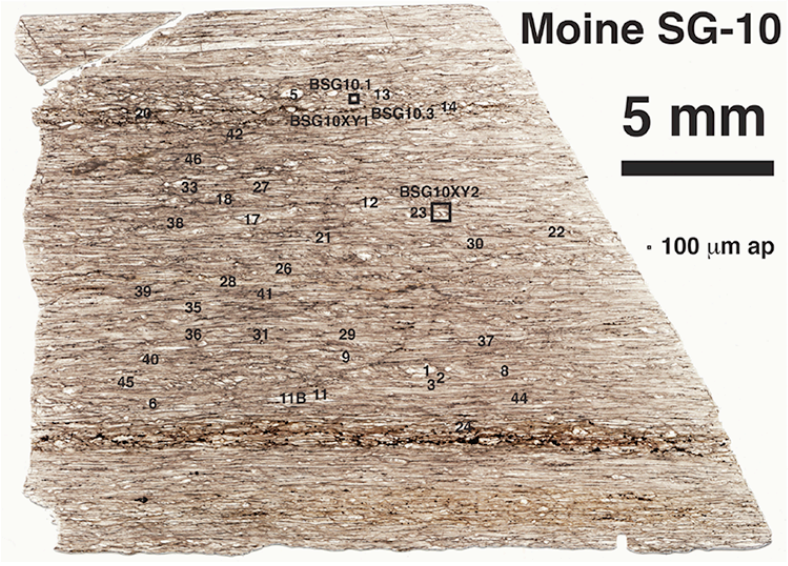

Fig. 1b

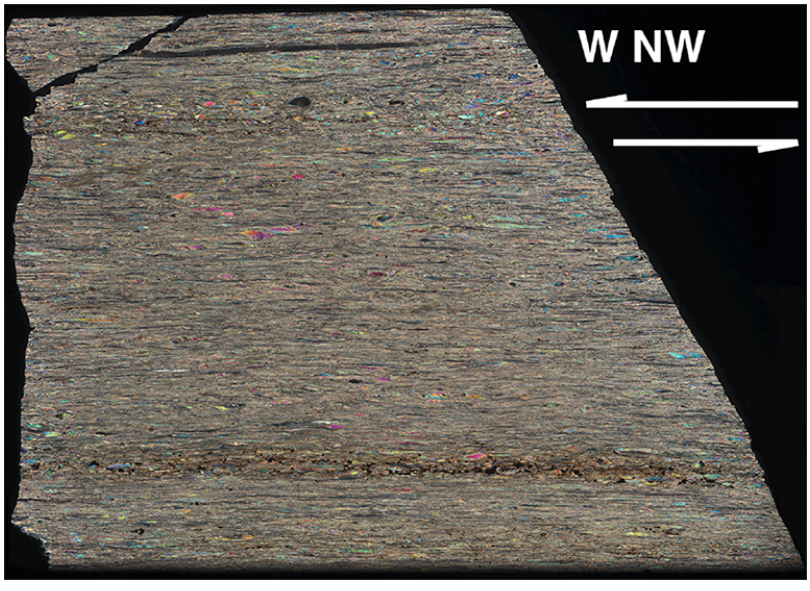

Solid Earth Discuss., doi:10.5194/se-2017-23, 2017
Manuscript under review for journal Solid Earth
Discussion started: 30 March 2017

Solid Earth
Discussions
Open Access
EGU

Fig. 1c

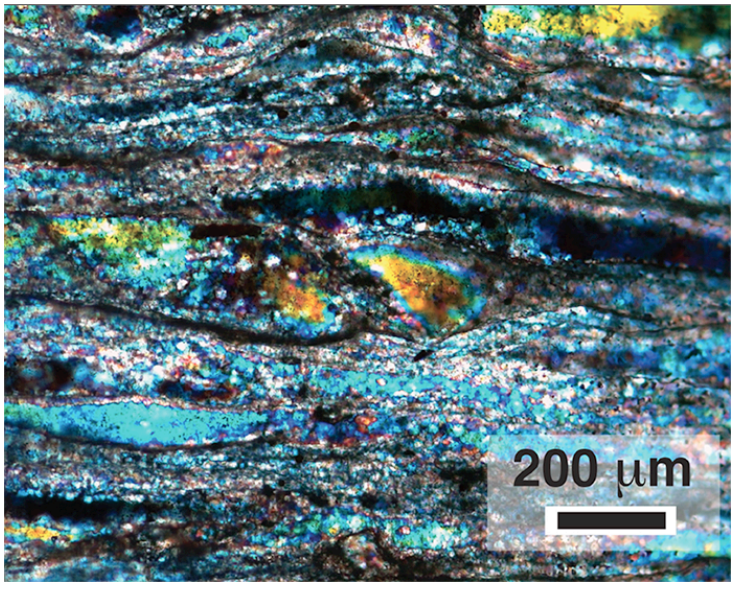

Fig. 1d

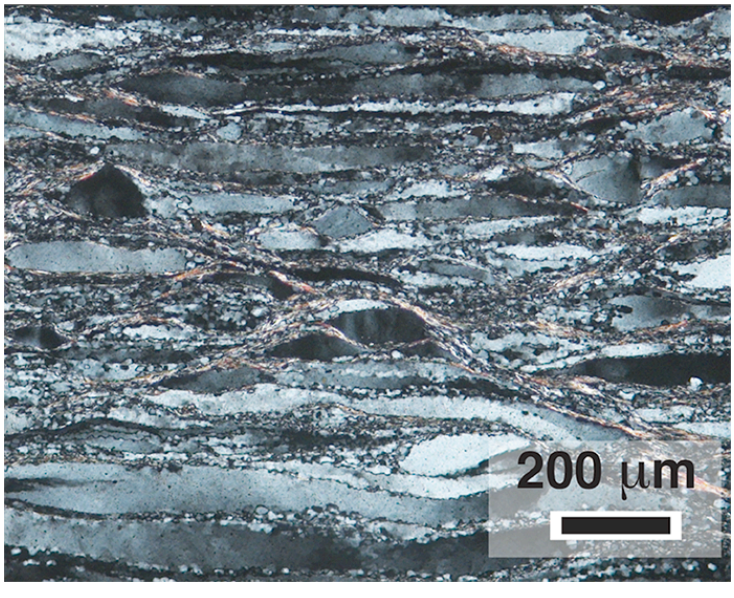

Solid Earth Discuss., doi:10.5194/se-2017-23, 2017
Manuscript under review for journal Solid Earth
Discussion started: 30 March 2017

Fig. 1e

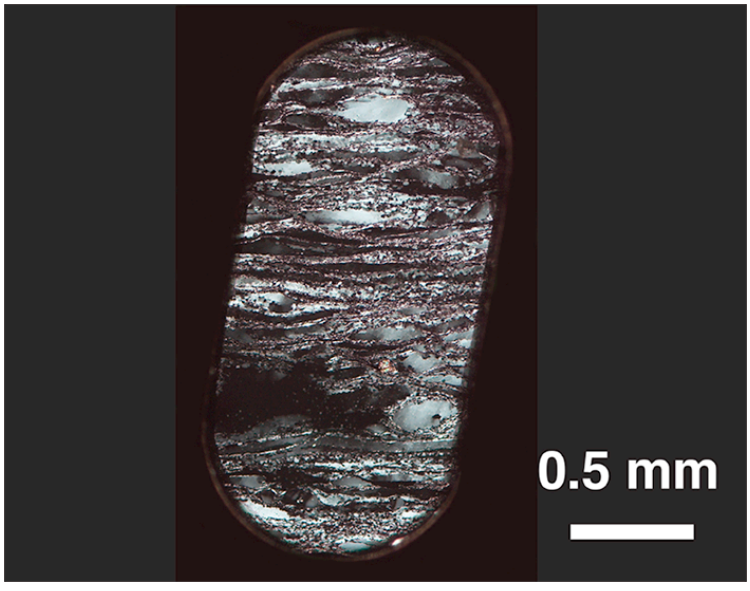

Fig. 1f

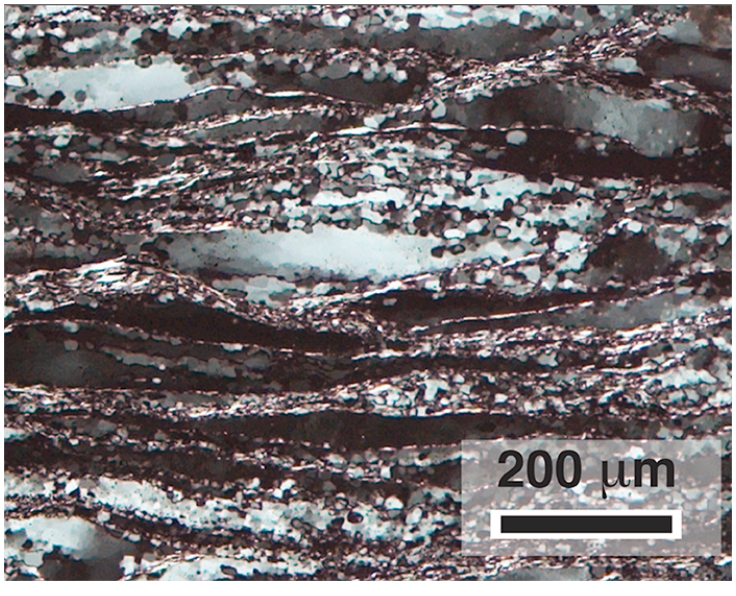

Solid Earth Discuss., doi:10.5194/se-2017-23, 2017
Manuscript under review for journal Solid Earth
Discussion started: 30 March 2017

Fig. 2a

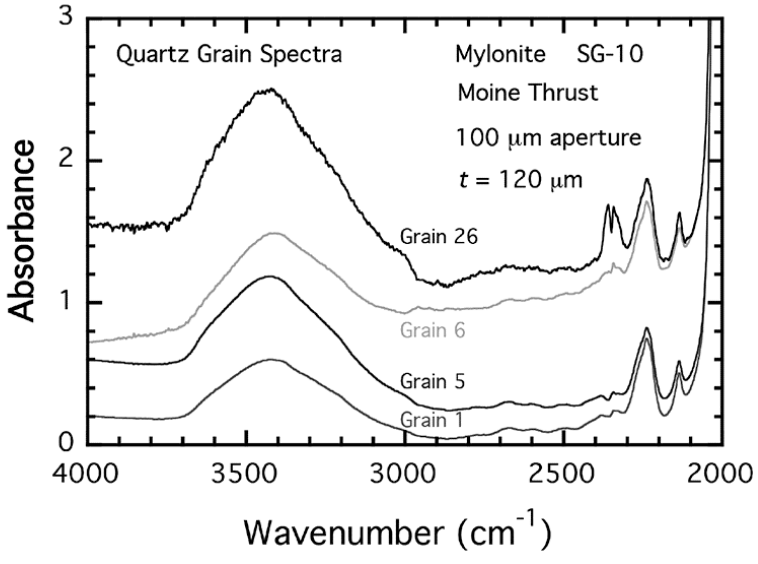

Fig. 2b

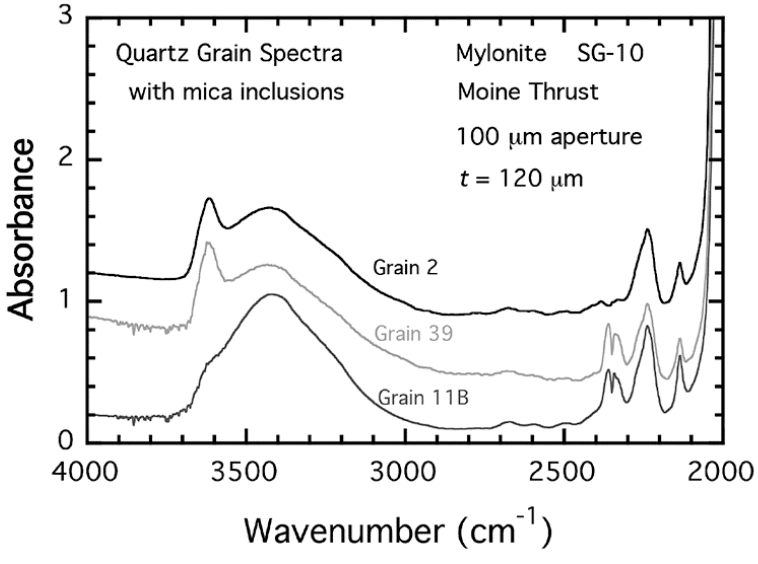

Solid Earth Discuss., doi:10.5194/se-2017-23, 2017
Manuscript under review for journal Solid Earth
Discussion started: 30 March 2017

Fig. 2c

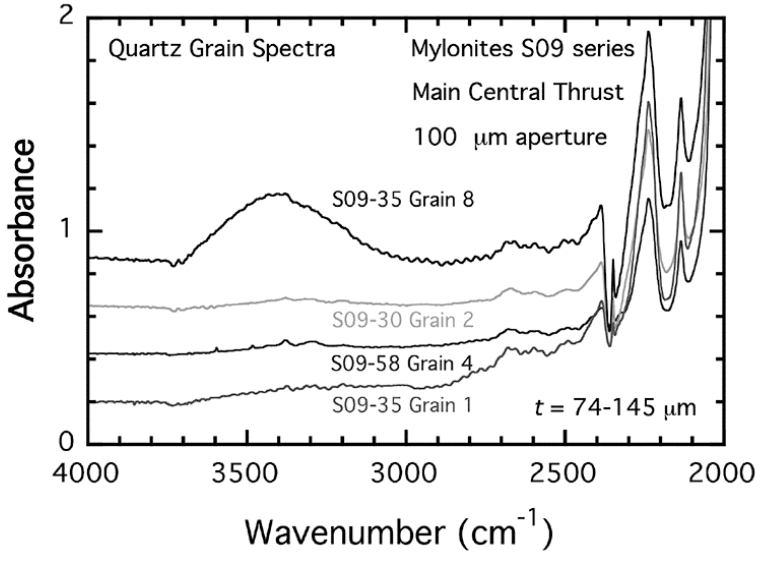

Fig. 2d

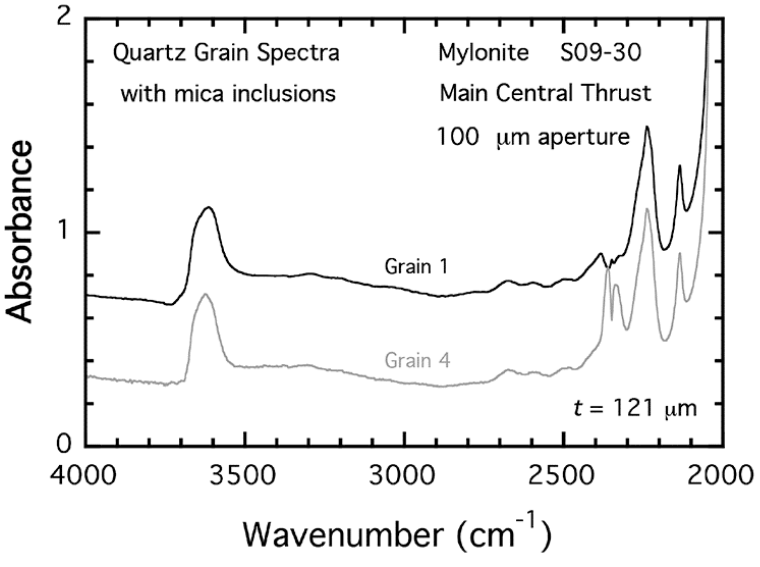

Solid Earth Discuss., doi:10.5194/se-2017-23, 2017
Manuscript under review for journal Solid Earth
Discussion started: 30 March 2017

Fig. 3a

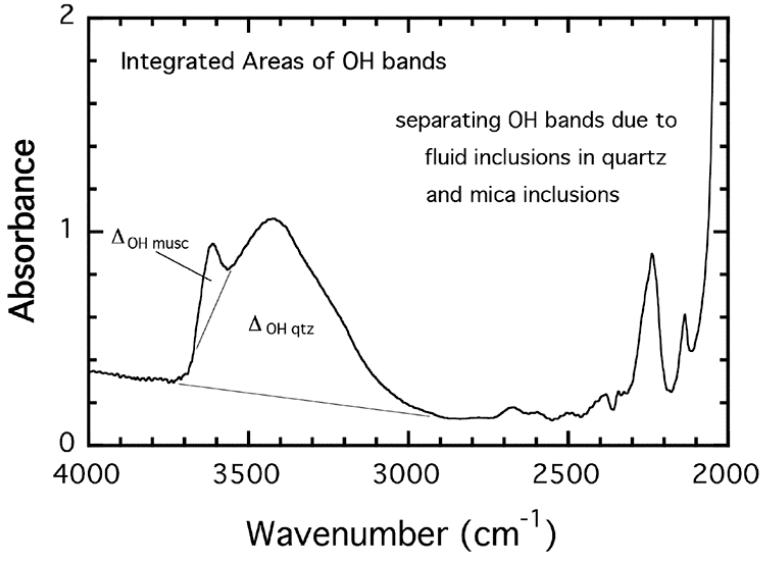

Fig. 3b

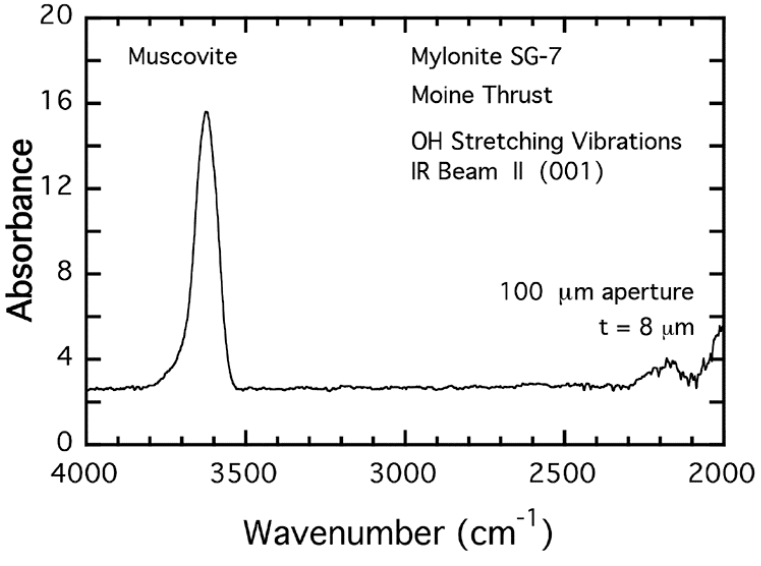

Solid Earth Discuss., doi:10.5194/se-2017-23, 2017
Manuscript under review for journal Solid Earth
Discussion started: 30 March 2017

Fig. 3c

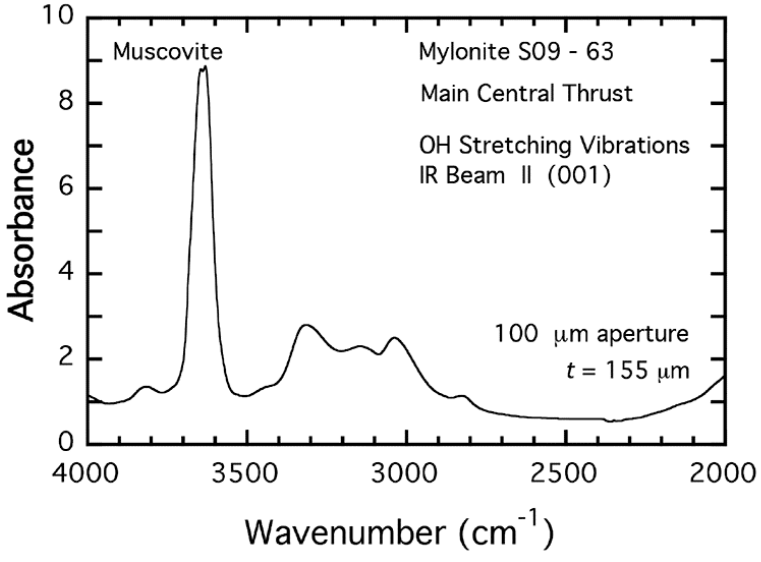

Fig. 3d

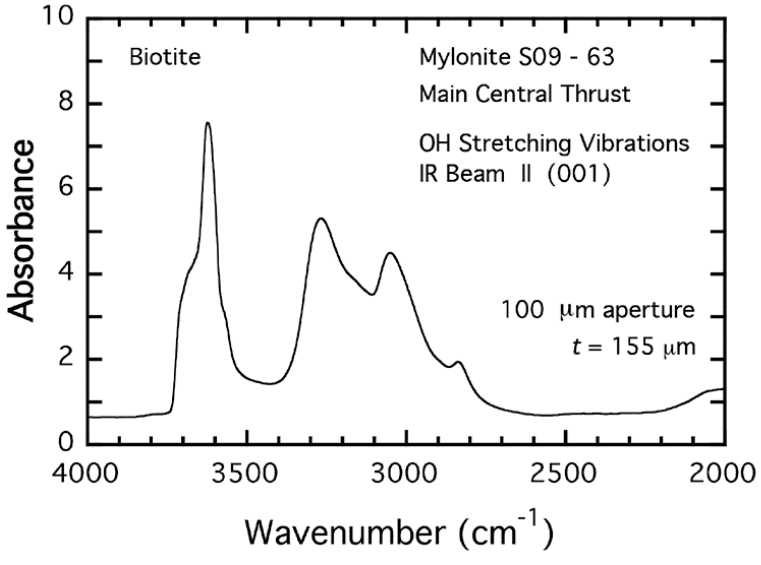

Solid Earth Discuss., doi:10.5194/se-2017-23, 2017
Manuscript under review for journal Solid Earth
Discussion started: 30 March 2017

Fig. 4a

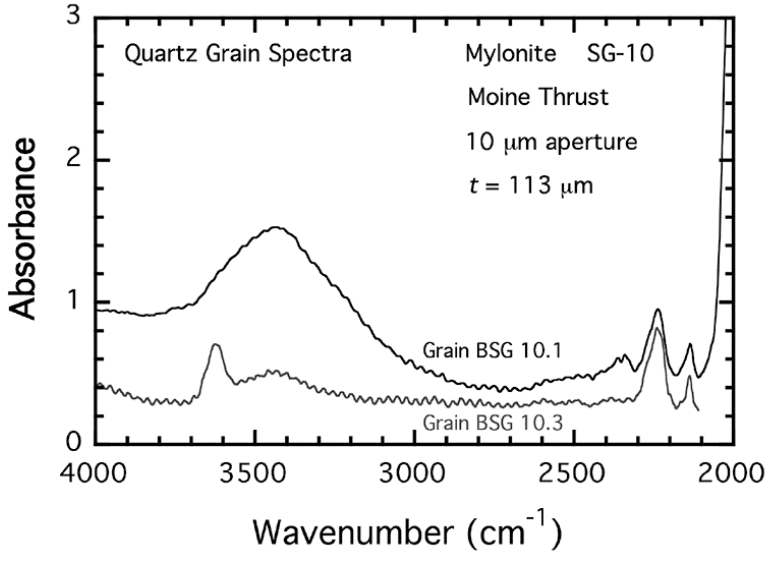

Fig. 4b

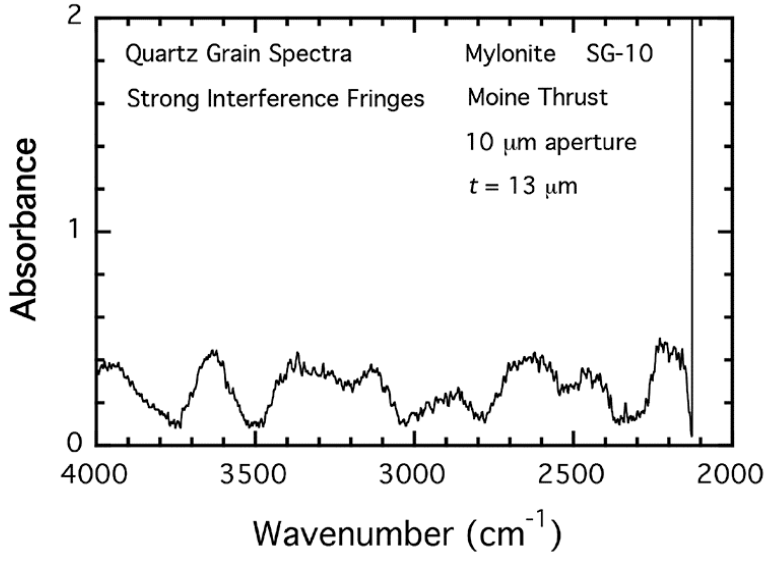

Solid Earth Discuss., doi:10.5194/se-2017-23, 2017
Manuscript under review for journal Solid Earth
Discussion started: 30 March 2017

Fig. 4c

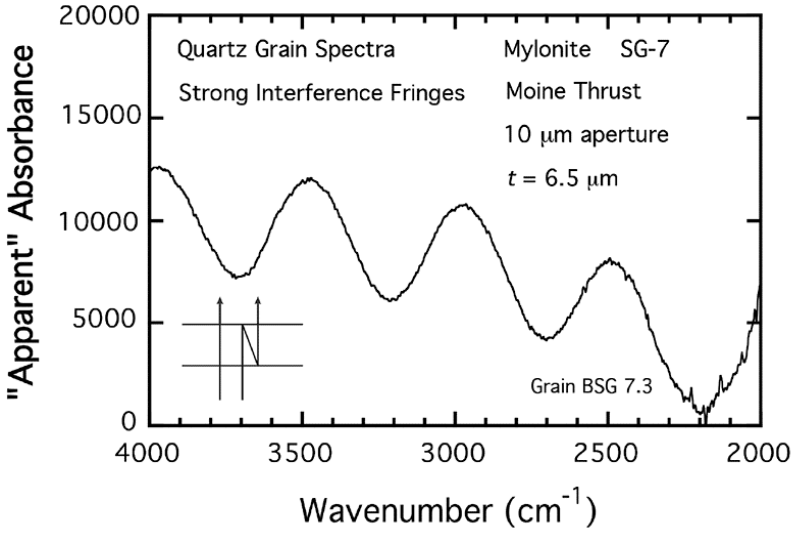

Solid Earth Discuss., doi:10.5194/se-2017-23, 2017
Manuscript under review for journal Solid Earth
Discussion started: 30 March 2017

Solid Earth
Discussions
Open Access
EGU

Fig. 5a

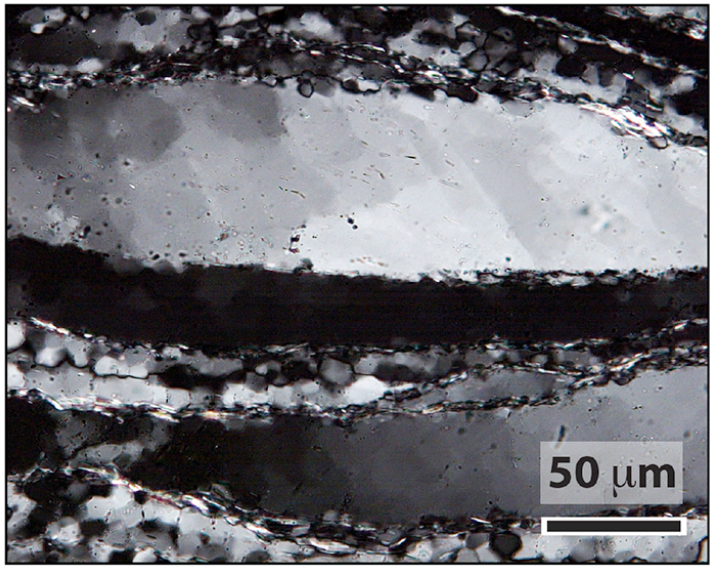

Fig. 5b

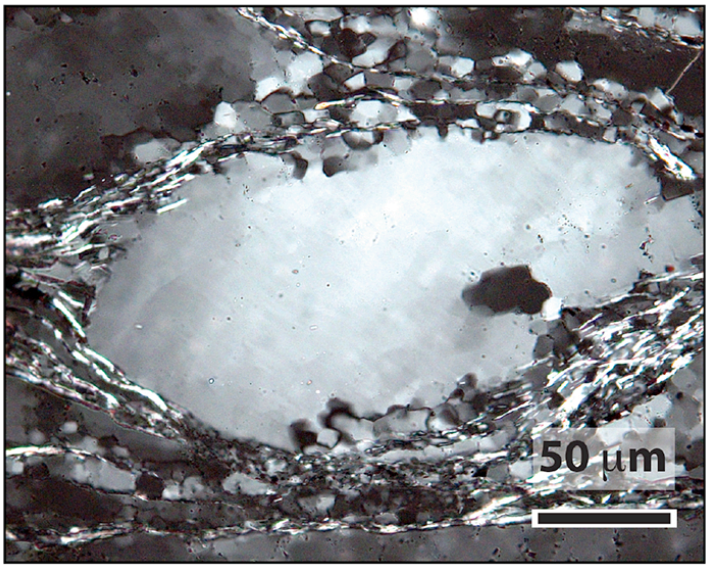

Solid Earth Discuss., doi:10.5194/se-2017-23, 2017
Manuscript under review for journal Solid Earth
Discussion started: 30 March 2017

Solid Earth
Discussions
Open Access
EGU

Fig. 6

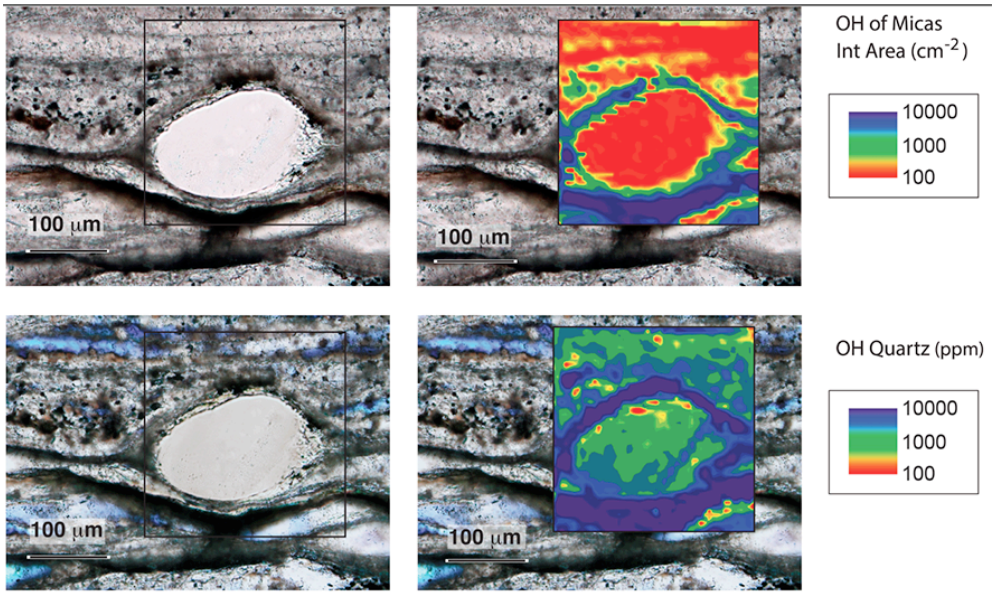

SG-7

Fig 7

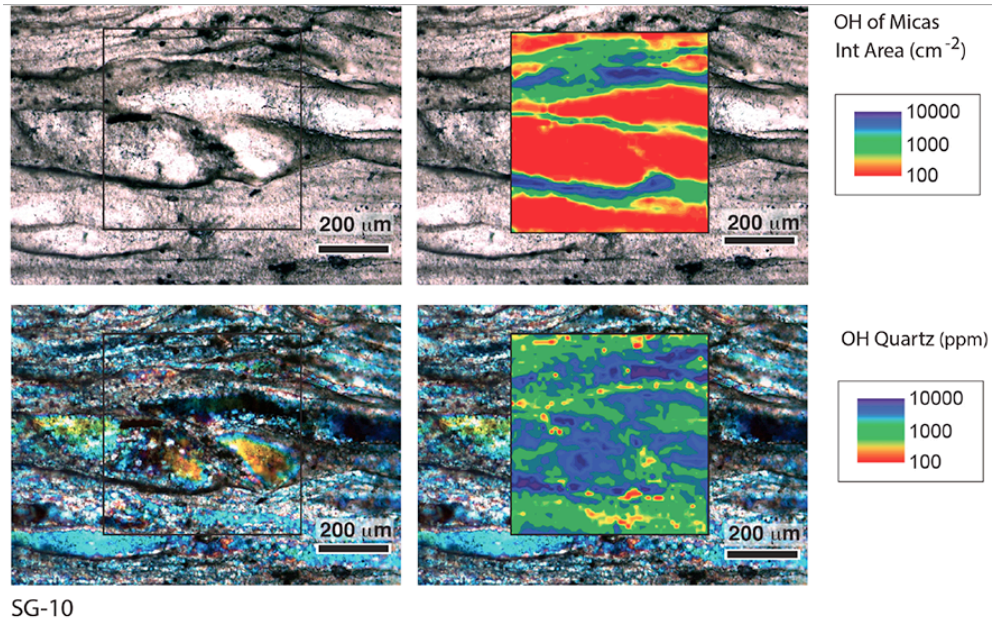

SG-10

Solid Earth Discuss., doi:10.5194/se-2017-23, 2017
Manuscript under review for journal Solid Earth
Discussion started: 30 March 2017

Fig. 8

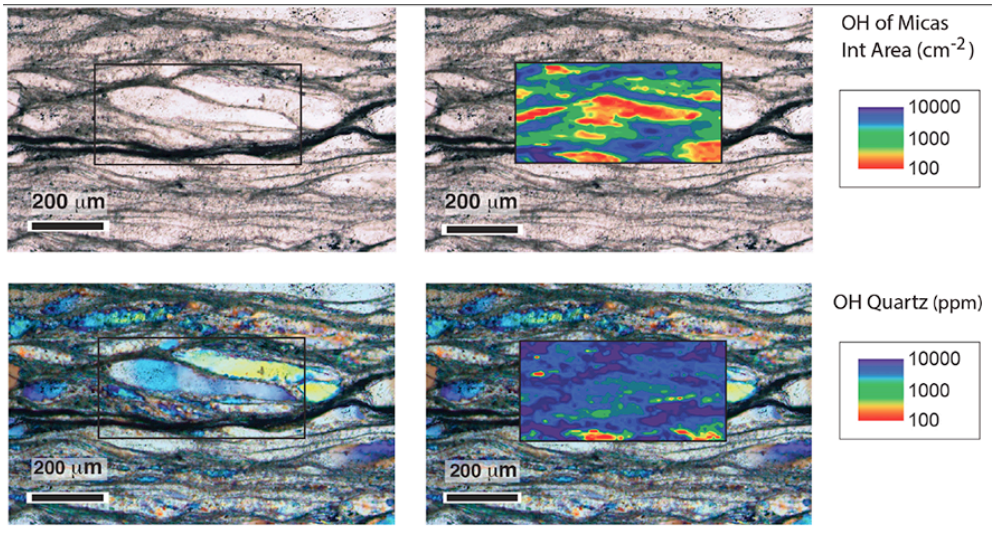

SG-8

Fig. 9

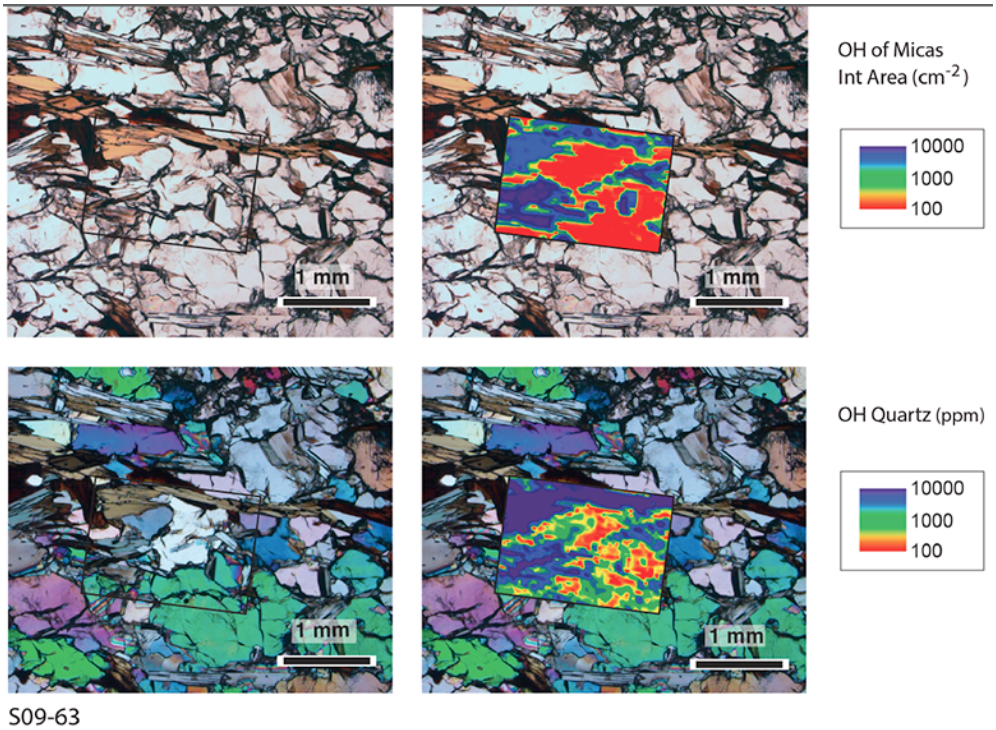

S09-63